Quaternary Science Reviews 198 (2018) 37–55

Contents lists available at ScienceDirect

Quaternary Science Reviews

journal homepage: www.elsevier.com/locate/quascirev

Hominin distribution in glacial-interglacial environmental changes in the Qinling Mountains range, central China

Xuefeng Sun [a, *], Huayu Lu [a], Shejiang Wang [b, c, **], Xinghua Xu [a], Qingxuan Zeng [a], Xuehe Lu [a], Chengqiu Lu [d], Wenchao Zhang [e], Xiaojian Zhang [a], Robin Dennell [f]

[a] School of Geography and Ocean Science, Nanjing University, Nanjing, 210023, China
[b] Key Laboratory of Vertebrate Evolution and Human Origins, Institute of Vertebrate Paleontology and Paleoanthropology, Chinese Academy of Sciences, Beijing, 100044, China
[c] CAS Center for Excellence in Life and Paleoenvironment, Beijing, 100044, China
[d] Hubei Provincial Institute of Cultural Relics and Archaeology, Wuhan, 430077, China
[e] Institute of Geology and Geophysics, Chinese Academy of Sciences, Beijing, 100029, China
[f] Dept. of Archaeology, University of Exeter, Exeter, EX4 4QE, UK

A R T I C L E I N F O

Article history:
Received 6 June 2018
Received in revised form
12 August 2018
Accepted 13 August 2018
Available online 5 September 2018

Keywords:
Qinling mountain range
Paleolithic sites
Loess–paleosol sequence
Human occupation
Climate change
Refugium

A B S T R A C T

The Qinling Mountain Range (QMR) in central China encompasses innumerable Paleolithic sites. The hominin settlement in the QMR is comparable with that in the Nihewan Basin in northern China. The recorded information on the loess deposition in the QMR include both hominin remains and environmental changes. Since 2004, geological, geomorphological, archaeological, and chronological investigations were conducted by our team. By systematically using luminescence, paleomagnetic, and $^{26}Al/^{10}Be$ burial dating methods to obtain age controls, and by correlating the pedostratigraphy and magnetic susceptibility of the Luochuan loess section, we established the loess–paleosol sequence and chronology of the lithic artifact levels for 35 Paleolithic sites and spots in the QMR. This work remarkable found shifts from glacial-to interglacial-driving hominin settlement patterns. During the stage between 1.2 and 0.7 Ma, large drying events, such as L15 (MIS 38) and L9 (MIS 22, 23 and 24), may have driven hominin migrations when the Loess Plateau was depopulated; moreover, the southern QMR was a glacial refugium. During the stage after ~0.60 Ma, the contrasts between glacial and interglacial scales are the greatest; furthermore, longer and warmer humid interglacial environments were dominant. S5 (MIS 13, 14, 15) and S1 (MIS 5) interglacial periods provided the optimal environments for hominin settlement and dispersal. On the basis of investigations, we also found that the hominin settlement is relatively continuous from ~1.20 Ma to ~0.05 Ma in the QMR. The human occupation of the QMR decreased considerably after ~0.05 Ma, probably because of changes in climate and human adaptations.

1. Introduction

Over the last two decades, important progress has been made in the discoveries, studies, and dating of the Chinese Paleolithic (e.g., Gao, 1999; Hou et al., 2000; Zhu et al., 2001, 2004; Gao and Hou, 2002; Wang and Huang, 2002; Wang et al., 2004, 2005; Deng et al., 2008; Wang et al., 2008a,b; Shen et al., 2009; Lu et al., 2007, 2011a; 2011b, 2017; Sun et al., 2012, 2013; Gao, 2013; Pei et al., 2015; Zhu et al., 2018; Zhang et al., 2018). Major achievements have also been made in the studies on the loess and paleosol sequence in China (e.g., Liu, 1985; An et al., 1990; Ding et al., 2002; Lu et al., 1999). This sequence is particularly important because it records not only the climate changes but also the Paleolithic artifacts and fossil hominin remains in the area (Liu and Ding, 1984, 1999; An and Ho, 1989; Ranov, 1995; Liu, 1999; Xia et al., 1999; Huang, 2000; Xiao et al., 2002; Yang et al., 2005; Lu et al., 2007; Du et al., 2008). Loess-covered Paleolithic sites are therefore important for studying the relationship between Paleolithic settlement and climate change.

* Corresponding author.
** Corresponding author. Key Laboratory of Vertebrate Evolution and Human Origins, Institute of Vertebrate Paleontology and Paleoanthropology, Chinese Academy of Sciences, Beijing, 100044, China.
E-mail addresses: xuefeng@nju.edu.cn (X. Sun), wangshejiang@ivpp.ac.cn (S. Wang).

https://doi.org/10.1016/j.quascirev.2018.08.012
0277-3791/

Studies on the climatic context of particular Paleolithic sites in China (e.g., Xia et al., 2001, 2008; Gao et al., 2008; Pei et al., 2009; Zhang and Chen, 2013; Li et al., 2014a; Ji et al., 2005; Li et al., 2016a,) and on earth surface processes and human evolution (e.g., Lu et al., 2017) have been conducted, but only a few of them have focused on long-term responses of Paleolithic societies to several glacial–interglacial shifts. The Qinling Mountain Range (QMR) in central China is one of those areas where this type of investigation is possible. The QMR encompasses ca. 400 Paleolithic sites and spots (i.e., "spots" refer to sites with lithic discoveries but no excavation was conducted). In particular, 30 Paleolithic sites and spots were identified in the Lantian area from 1963 to 2009 (Wang et al., 2014a), 268 Paleolithic sites and spots were found in the Luonan Basin between 1995 and 2004 (Shaanxi Provincial Institute of Archaeology, 2007), 52 Paleolithic sites and spots were found in the Danjiangkou area in 1994 (Li et al., 2009), and a 43 Paleolithic sites and spots were recorded in the Danjiangkou area in 2004 (Li et al., 2012). These sites and spots have been found to occur in the Early, Middle, and Late Pleistocene climatic contexts. Therefore, the QMR is a potential target area for studying how hominin societies responded to glacial–interglacial climate and environmental changes.

Before our investigations, the only sites in the QMR that had been dated were the Lantian hominin (Gongwangling) and Chenjiawo sites (An and Ho, 1989) and the Longyadong Cave (Wang and Huang, 2002). Since 2004, systematic geological, geomorphological, archaeological, and chronological investigations have been conducted by a joint team from Nanjing University, the Institute of Vertebrate Paleontology and Paleoanthropology (IVPP), Beijing, of the Chinese Academy of Sciences, and the Shaanxi Provincial Institute of Archaeology in the QMR.

2. Geologic and geomorphologic setting

Since the Cenozoic period, several fault basins have formed in the QMR, such as the Hanzhong, Ankang, and Luonan basins (Zhang, 1981; Xia, 1984). Tertiary red sandstone, siltstone, and mudstone were deposited in most basins. During the Quaternary period, eolian loess was deposited in all these basins to combine with eolian deposit. The rivers in these basins were dominated by erosion, and multistage terraces developed along rivers. These terraces were then covered with several meters of loess.

The Qinling Mountains act as a collective natural barrier, and it depicts the boundary between the southern and northern climatic regimes of China, a sensitive area of climate change controlled by the East Asian Monsoon (EAM). The Loess Plateau is situated to the north of the Qinling Mountains (Fig. 1). Loess deposition in the Loess Plateau has been on a massive scale, reaching 300 m in the northwest, 175 m in the central part, 130 m in the Lantian area in the northern Qinling Mountains, and 100 m–30 m in the eastern and southern part of Qinling Mountains. The climate varies from arid to semi-arid and semi-humid. The Qinling Mountains can block most of the dust transport from northwest to southeast China, consequently lessening the loess deposition in the QMR basins. Compared with those in the Loess Plateau, the loess is thinner, the grain size is finer, the sedimentation rate is lower, and the color is considerably more reddish in the QMR, but it can still be correlated with the classic Luochuan loess–paleosol sequence (Lu et al., 2007, 2012; 2017; Zhang et al., 2012; Sun et al., 2012; 2104, 2016; 2017a, 2017b).

In the QMR, the South Luohe River originates in the Luonan Basin in the eastern Qinling Mountains, flows through several basins, and joins the Huang He (Yellow River) in Luoyang. The Hanjiang River and its main branches originate from the southern slopes of the Qinling Mountains, flow through several basins, and join the Yangtze River in Wuhan. The Bahe River originates from the northern slopes of the Qinling Mountains and joins the Weihe River in Xi'an. Although the Qinling Mountains are an obvious natural barrier between northern and southern China, the rivers that flow through them also provide several natural corridors for the humid and sub-tropical regions of southern China and the temperate and semi-arid regions of northern China.

According to the elevation measurements of the bedrock and gravel layers of the terraces along the abovementioned rivers by using the Trimble R8 GNSS system, and on the basis of previous investigations (e.g., Shen, 1956; Lu et al., 2017), we set up a three-terrace system along the Bahe and South Luohe River Valleys and a five-terrace system along the Hanjing River Valley.

3. Archeological setting

Paleolithic artifacts have been found in the Luonan and Lushi basins along the South Luohe River Valley in eastern QMR (Fig. 2B), in the Hanzhong, Ankang, and Yunxian basins and the Danjiangkou area along the Hanjiang River Valley in southern QMR (Fig. 2C), and in Lantian area along the Bahe River Valley in northern QMR (Fig. 2A).

3.1. South Luohe River Valley

Eight Paleolithic sites and spots (Shizilukou, Zhanghuokou, Mengwa, Guoyan, Liuwan, Sangbaichuan, and the Longyadong Cave sites in Luonan Basin, and Qiaojiayao Paleolithic site and Zhuangzicun Paleolithic spots in the Lushi Basin) were excavated and discovered by our team (Fig. 2B).

Nearly 77,000 lithic artifacts were excavated in the Longyadong Cave site (Shaanxi Provincial Institute of Archaeology, 2007) from 1995 to 1997. Thousands of lithic artifacts were excavated in Shizilukou (3538) (Xing, 2014), Zhanghuokou (unpublished), and Guoyan (unpublished). Hundreds of lithic artifacts were excavated in Mengwa (unpublished), Qiaojiayao (880), and Liuwan (216) (Lu et al., 2007, 2011a; 2012; Sun et al., 2014). Several lithic artifacts were also collected at the Zhuangzicun spot (Wang et al., 2008a). All these sites and spots along the South Luohe River have been dated (Wang and Huang, 2002; Lu et al., 2007, 2011a; b; 2012; Sun et al., 2013, 2014; Wang et al., 2008a; Wang and Lu, 2016).

3.2. Hanjiang River Valley

Five Paleolithic sites and spots (Hejialiang, Yaochangwan, Longgangsi-1, Longgangsi-2, and Longgangsi-3) were found in the Hanzhong Basin, two Paleolithic spots (Luojiacun and Wutaicun) were discovered in the Ankang Basin, and two Paleolithic sites (Dishuiyan and Houfang) in the Yunxian Basin were excavated by our team long the Hanjiang River (Fig. 2C).

Thousands of artifacts at Longgangsi-1 (unpublished), Longgangsi-3 ($N = 4441$) (Xia et al., 2018), and Longgangsi-2 ($N = 83$) (Sun et al., 2017a) were excavated. Hundreds were also scientifically excavated at Houfang ($N = 162$) (Li et al., 2014b), Dishuiyan ($N = 600$) (Liu and Feng, 2014), and Hejialiang ($N = 252$) (Wang et al., 2014b). Several artifacts were discovered at the Yaochangwan, Luojiacun, and Wutaicun spots. All these Paleolithic sites and spots along the Hanjiang River have been dated (Sun et al., 2012; 2017a; Wang and Lu, 2016; Li et al., 2016b).

3.3. Bahe River Valley

Ten Paleolithic spots, including those in Jijiawan, Diaozhai, and Ganyugou in the Lantian area, were found and artifacts were collected by our team (Fig. 2A). Hundreds of artifacts in Ganyu

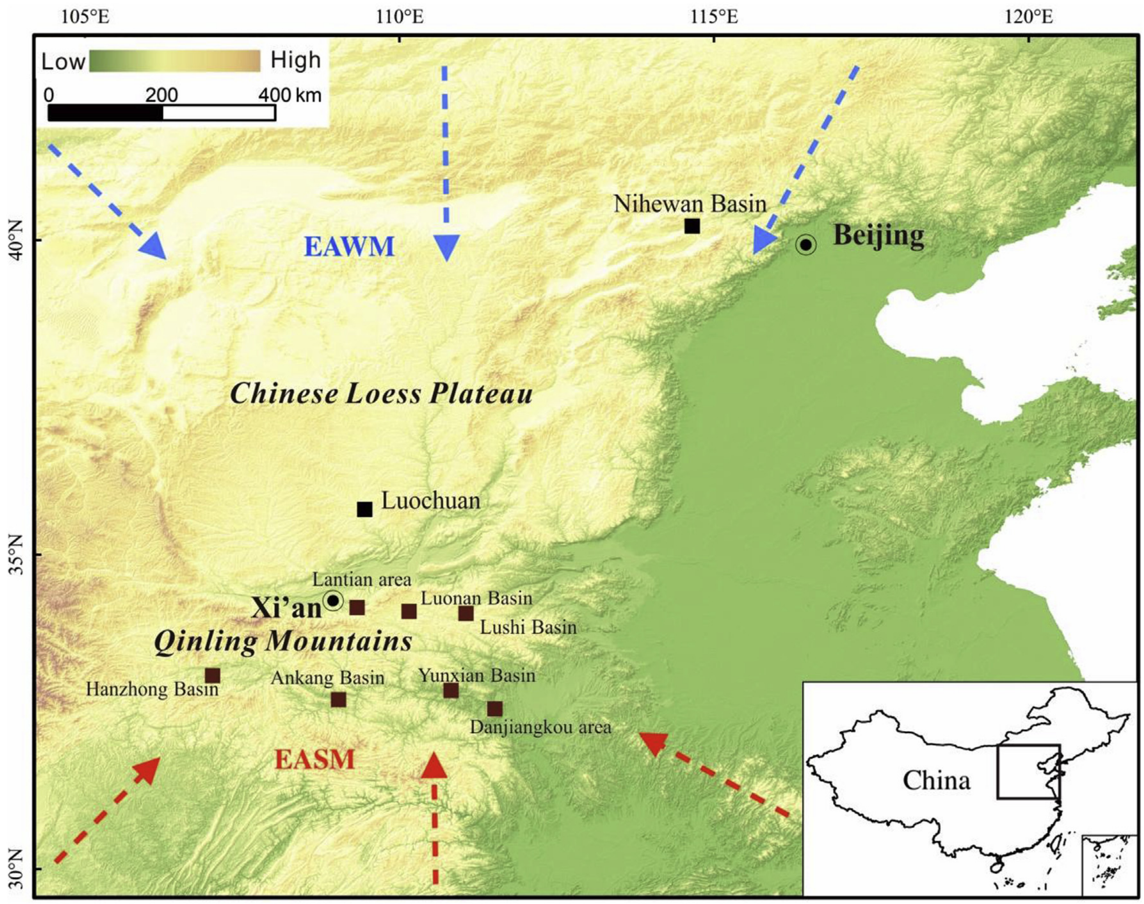

Fig. 1. Locations of investigated Luonan, Lushi, Hanzhong, Ankang, and Yunxian Basins and Lantian and Danjiangkou areas (brown square); relevant loess section in the Nihewan Basin and Luochuan (black square); East Asian Winter Monsoon (EAWM) (blue arrows); and East Asian Summer Monsoon (EASM) (red arrows). (For interpretation of the references to color in this figure legend, the reader is referred to the Web version of this article.)

(N = 550) (Wang et al., 2014a) and Diaozhai (N = 114) were collected, respectively. Several artifacts were also discovered in Jijiawan. We had also dated these three Paleolithic spots along the Bahe River (Wang et al., 2014b; Wang and Lu, 2016; Zhuo et al., 2016).

4. New discoveries from 2015 to 2017

With regard to the new investigations conducted from 2015 to 2017 along the Hanjiang River Valley in the southern Qinling Mountains, we searched for exposed loess sections containing lithic artifacts on the Hanjiang River terraces. After searching and examining hundreds of exposed loess sections, we found ten new Paleolithic spots (Fig. 3): Yangjiaping, Liangshancun, Lianfengcun-1, Liangfengcun-2, and Erligou in the Hanzhong Basin, Qujiahe, Shuanghongcun, and Chihe in the Ankang Basin, and Wujiagou and Jiuchang in the Yunxian Basin (Table 1).

5. Multi-dating methods

The main methods for dating Chinese loess and paleosol sequences are optically stimulated luminescence (OSL), paleomagnetism and pedostratigraphic correlation for the type section of the Luochan loess–paleosol sequence on the central Chinese Loess Plateau (CLP). Nevertheless, because the dose rate of quartz in Chinese loess is ~200 Gy (e.g., Buylaert et al., 2007), it is not possible to date loess samples >0.1 Ma by using the initial part of the OSL signal. Therefore, if one relies only on OSL and the paleomagnetic Matuyama–Brunhes boundary (0.78 Ma) as a marker horizon, then there is a blind area between ~ 0.1 Ma and ~0.78 Ma.

Thermally transferred OSL (TT-OSL) (Wang et al., 2006, 2007; Stevens et al., 2009; Sun et al., 2010, 2013; Yi et al., 2012) and K-feldspar post-infrared (IR) IR-stimulated luminescence (post-IR IRSL; pIRIR$_{290}$) (Thomsen et al., 2008; Murray et al., 2009; Li and Li, 2011; Buylaert et al., 2012; Yi et al., 2015; Sun et al., 2017c) can potentially extend the age range beyond the current limits of OSL. Accordingly, both methods can extend the dating age range of the QMR loess. For example, the TT-OSL age of the loess at the Houfang Paleolithic site is extended to ~0.18 Ma (Sun et al., 2016; Li et al., 2016b), while that at the Longyadong Cave is ~0.39 Ma (Sun et al., 2014).

$^{26}Al/^{10}Be$ burial dating is a relatively new radio-isotopic dating method based on the buildup and radioactive decay of two cosmogenic nuclides. The dating range of this method is ~0.3–5.0 Ma (Shen, 2012). When using simple $^{26}Al/^{10}Be$ burial dating, we can obtain the minimum burial age if the thickness of the loess cover is not > 10 m. We dated the vein quartz lithic artifacts from the Liuwan Paleolithic site and obtained the minimum age of ~0.6 Ma (Wang et al., accepted), and then we dated the gravels on the sixth Hanjing terrace at the Hanzhong Basin, which is older than ~1.5 Ma, and the gravels on the fifth Hanjing terrace at the Yunxian Basin, which is older than ~2.0 Ma (Xu et al., in review).

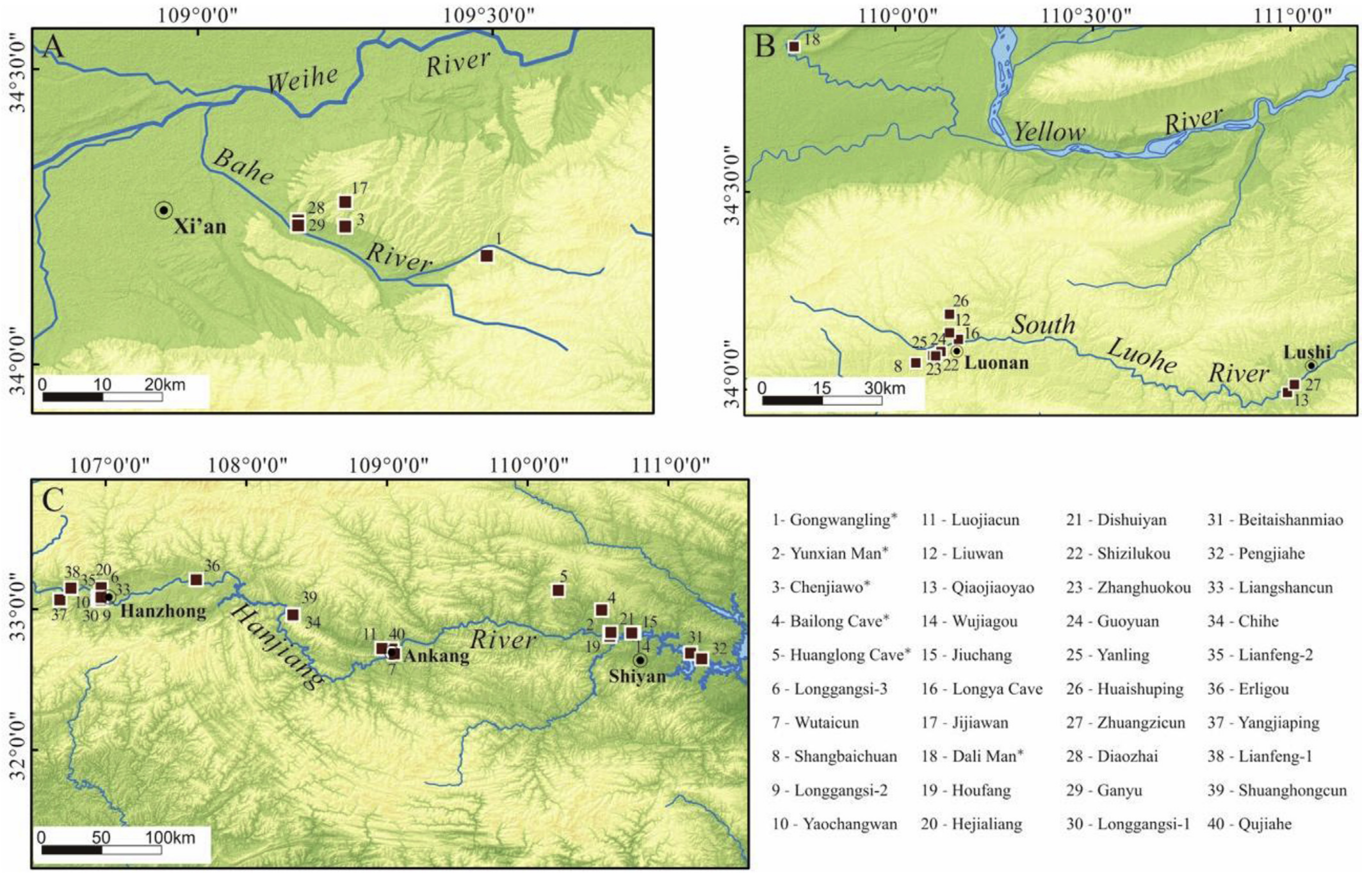

Fig. 2. Locations of our discovered and dated Paleolithic sites and spots and other relevant sites (*) along the Bahe River (A), South Luohe River (B), and Hanjiang River (C) in the QMR. (Numbering sequences of 40 Paleolithic sites and spots are the same as those in Figs. 2 and 4 and Table 3.)

By systematically using OSL, TT-OSL, post-IR IRSL, $^{26}Al/^{10}Be$ burial dating, and paleomagnetic dating methods to obtain the age controls, and by deriving the correlation of pedostratigraphy, magnetic susceptibility, and chronology (Lu et al., 1999; Ding et al., 2002) of the Luochuan loess section, we managed to date every loess section at the Paleolithic sites.

Loess samples dated by OSL, TT-OSL, and K-rich feldspar $pIRIR_{290}$ ages provide tightly established age data (Table 2). The Paleolithic spots of Yangjiaping, Liangshancun, Liangfengcun-1, Liangfengcun-2, Erligou, Shuanghongcun, and Chihe are on the second Hanjiang river terrace covered by thin loess deposits. The Qujiahe spot is on the third Hanjiang river terrace covered by a thin loess deposit. We therefore used OSL, TT-OSL, post-IR IRSL methods, and then applied the TT-OSL method in dating these eight new Paleolithic sites. The dating results are listed in Table 2. The dating age ranges are ~0.05 Ma to ~0.20 Ma. After correlating the pedostratigraphy and magnetic susceptibility of the Luochuan loess section, these Paleolithic artifact levels are in the S1, L2, and S2 layers of the loess sections that correspond to MIS 5, 6, and 7, respectively.

The Wujiagou and Jiuchang spots are on the third Hanjiang river terrace and were covered by thick loess sections. We used TT-OSL, post-IR IRSL, $^{26}Al/^{10}Be$ burial dating, and paleomagnetic dating methods to obtain age controls, and then we derived the correlation between magnetic susceptibility and chronology of the Luochuan loess section (Lu et al., 1999; Ding et al., 2002). Both Wujiagou and Jiuchang are in the S5 layer (MIS 13, 14, and 15) with an age range of ~0.58–0.47 Ma (Table 3).

6. Chronology of Paleolithic artifact levels

On the basis of the latest report on the Shangchen site, the earliest evidence of hominin occupation of the QMR is from 2.12 Ma to 1.26 Ma in Lantian (Zhu et al., 2018). The second oldest site is the Gongwangling site, in which the age of the paleosol S22 or S23 layer (MIS 53 or 55) is ~1.63 Ma, also in Lantian (Fig. 4 and Table 3) (Zhu et al., 2015). The third oldest site is the Longgangsi Paleolithic site, in which the age of the L15 layer (MIS 38) is ~1.2 Ma (Fig. 4 and Table 3) in the Hanzhong Basin (Sun et al., 2017a).

The loess layers with thicknesses of 8 m at Longgangsi-3 are dated from ~1.26 Ma to ~0.76 Ma, and they correspond to L15 (MIS 38) to S7 (MIS 19) layers. A thin Paleolithic artifact level at Wutaicun is in the S9 layer (MIS 25 and 26) (Sun et al., 2017a) with an age range of ~0.88–0.85 Ma (Lu et al., 1999). In the excavation trench (newly tested) which is within 1 km away from the Yunxian hominin (Xuetangliangzi) site, we found Paleolithic artifacts distributed throughout the loess section from top to bottom. We also dated this new loess section by using paleomagnetic dating. This method produced the same result as that at the Xuetangliangzi loess section (De Lumley and Li, 2008; Bahain et al., 2017). Therefore, the thick Paleolithic artifact level at the Yunxian hominin site corresponds to L9 (MIS 22, 23, and 24), S8 (MIS 21), L8 (MIS 20), and S7 (MIS 19) layers with age ranges of ~0.85–0.71 Ma based on the

Fig. 3. Newly discovered spots and artifact levels in-situ with exposed loess sections along the Hanjiang River Valley (2015–2017). a: Erligou; b: Lianfengcun-1; c: Shuanghongcun; d: Wujiagou; e: Jiuchang; f: Liangfengcun-2; g: Yangjiaping; h: Qujiahe; i: Liangshancun.

Table 1
Newly discovered Paleolithic spots in the Hanjiang River Valley (2015–2017).

Basin	Site	Artifacts in section	Artifacts on surface	Total	Artifact depth	Types
Hanzhong Basin	Yangjiaping	8	16	24	160 cm and 520 cm	cores, flakes, and chunks
	Liangshancun	38	0	38	50 cm and 355 cm	flakes, retouched scrapers, and flaking debris
	Lianfengcun-1	4	14	18	80 cm and 200 cm	cores, flakes, retouched scrapers, and chunks
	Lianfengcun-2	8	0	8	65 cm and 345 cm	cores, flakes, and flaking debris
	Erligou	9	30	39	150 cm and 450 cm	cores, flakes, retouched scrapers, and chunks
Ankang Basin	Qujiahe	27	0	27	110 cm and 280 cm	cores, flakes, and chunks
	Shuanghongcun	22	41	63	110 cm and 170 cm	cores, flakes, retouched scrapers, chunks, flaking debris
	Chihe	2	13	15	240 cm	flakes and chunks
Yunxian basin	Wujiagou	4	8	12	520–540 cm	flakes and chunks
	Jiuchang top	13	9 near section	24	1600 cm	cores, flakes, hand-axes, and chunks
	Jiuchang base	2			1550 cm	

Table 2
Summary of luminescence dating ages of Paleolithic sites and spots in the QMR, with sample codes, depth, radionuclide concentrations, dose rates, and OSL, TT-OSL, K-rich feldspar $pIRIR_{290}$ equivalent doses and ages. (*Ages of YL, GY, SZLK, and HSP sites previously mentioned by Wang and Lu (2014) Original OSL data published in this paper.).

Lab No.	Sample No.	U (ppm)	Th (ppm)	K (%)	WC (%)	De (Gy)	Dose rate (Gy/ka)	Age (ka)			Reference
								SAR-OSL	TT-OSL	pIRIR290	
NJU-2356	LSC-50	2.24 ± 0.09	12.9 ± 0.3612	2.00 ± 0.06	10.10	423 ± 13	3.03 ± 0.19		140 ± 10		This paper
NJU-2357	LSC-120	2.34 ± 0.10	13.6 ± 0.37	1.85 ± 0.06	10.70	566 ± 7	2.96 ± 0.17		191 ± 12		This paper
NJU-2362	LF-1-80	2.03 ± 0.09	12.80 ± 0.36	1.78 ± 0.06	9.77	182 ± 7	2.80 ± 0.18		65 ± 5		This paper
NJU-2364	LF-1-200	2.94 ± 0.11	13.00 ± 0.36	1.96 ± 0.06	11.71	466 ± 3	3.12 ± 0.15		150 ± 8		This paper
NJU-2366	LF-2-65	3.38 ± 0.12	13.60 ± 0.37	1.70 ± 0.06	12.14	343 ± 27	3.01 ± 0.13		114 ± 11		This paper
NJU-2367	LF-2-345	2.69 ± 0.10	12.9 ± 0.36	1.94 ± 0.06	7.19	523 ± 10	3.05 ± 0.27		172 ± 16		This paper
NJU-2369	YJP-170	2.77 ± 0.11	13.80 ± 0.37	1.72 ± 0.06	10.23	213 ± 16	2.93 ± 0.18		73 ± 7		This paper
NJU-2370	YJP-520	2.47 ± 0.10	12.90 ± 0.36	1.93 ± 0.06	14.34	346 ± 54	3.01 ± 0.08		115 ± 19		This paper
NJU-2372	ELG-170	2.93 ± 0.11	13.40 ± 0.38	1.90 ± 0.06	12.89	341 ± 14	3.17 ± 0.12		107 ± 6		This paper
NJU-2373	ELG-220	2.93 ± 0.11	13.4 ± 0.38	1.90 ± 0.06	16.44	389 ± 17	3.09 ± 0.05		126 ± 6		This paper
NJU-2376	CH-1-100	2.91 ± 0.11	13.2 ± 0.37	2.02 ± 0.06	13.83	304 ± 17	2.86 ± 0.09		106 ± 7		This paper
NJU-2377	CH-1-160	2.64 ± 0.10	15.00 ± 0.41	1.71 ± 0.06	15.62	448 ± 45	2.97 ± 0.06		151 ± 16		This paper
NJU-2378	CH-2-60	2.29 ± 0.09	14.40 ± 0.39	1.60 ± 0.05	13.47	310 ± 23	2.79 ± 0.09		111 ± 9		This paper
NJU-2379	CH-2-110	2.75 ± 0.11	15.2 ± 0.41	1.65 ± 0.05	18.03	462 ± 40	2.95 ± 0.05		157 ± 14		This paper
NJU-2383	QJH-100	2.88 ± 0.11	14.80 ± 0.40	1.57 ± 0.05	19.41	290 ± 20	2.88 ± 0.08		101 ± 8		This paper
NJU-2384	QJH-240	2.91 ± 0.11	14.90 ± 0.40	2.00 ± 0.06	11.22	421 ± 29	3.19 ± 0.25		132 ± 14		This paper
NJU-1658	YL-50	2.37 ± 0.10	13.7 ± 0.37	2.03 ± 0.06	14.50	299 ± 13	3.75 ± 0.17			80 ± 5	Wang and Lu 2014*
NJU-1661	YL-170	2.33 ± 0.10	16.3 ± 0.42	1.62 ± 0.06	26.11	>743	3.18 ± 0.13			>233	Wang and Lu 2014*
NJU-1480	GY-1	3.120.11	15.4 ± 0.42	2.08 ± 0.06	16.91	328 ± 11	3.56 ± 0.17		92 ± 6		Wang and Lu 2014*
NJU-1482	GY-2	3.20 ± 0.12	15.6 ± 0.42	1.94 ± 0.06	16.22	685 ± 81	3.47 ± 0.17		197 ± 26		Wang and Lu 2014*
NJU-1654	SZLK-1	2.86 ± 0.11	13.9 ± 0.38	2.19 ± 0.06	15.20	181 ± 15	3.68 ± 0.18		49 ± 5		Wang and Lu 2014*
NJU-1657	SZLK-2	2.89 ± 0.11	15.3 ± 0.40	1.97 ± 0.06	19.33	375 ± 33	3.36 ± 0.16		112 ± 12		Wang and Lu 2014*
NJU-347	HSP-1	2.18 ± 0.08	14.9 ± 0.39	1.98 ± 0.04	15.18	200 ± 19	3.46 ± 0.11	58 ± 6			Wang and Lu 2014*
NJU-348	HSP-2	2.23 ± 0.08	16.8 ± 0.42	1.73 ± 0.04	23.15	296 ± 19	3.31 ± 0.12	89 ± 7			Wang and Lu 2014*
NJU-1329	DSY-M	2.33 ± 0.09	14.4 ± 0.39	2.25 ± 0.07	15	158 ± 8	3.43 ± 0.18	45 ± 3			Sun et al., 2016
NJU-1330	DSY-B	2.18 ± 0.09	8.95 ± 0.28	1.43 ± 0.05	15	252 ± 17	3.37 ± 0.17	108 ± 9			Sun et al., 2016
NJU-1468	HF-1	3.11 ± 0.11	14.9 ± 0.40	2.09 ± 0.06	15	316 ± 26	3.70 ± 0.18		85 ± 8		Li et al., 2016a,b
NJU-1472	HF-5	2.61 ± 0.10	14.1 ± 0.39	1.750.06	15	417 ± 23	3.13 ± 0.16		133 ± 10		Li et al., 2016a,b
NJU-691	HJL-2	2.79 ± 0.10	13.1 ± 0.37	2.49 ± 0.07	15	310 ± 13	3.59 ± 0.22		86 ± 6		Sun et al., 2012
NJU-1690	JJW-2	2.45 ± 0.10	15.1 ± 0.39	1.84 ± 0.06	20	358 ± 12	3.46 ± 0.15			104 ± 6	Zhuo et al., 2016
NJU-2161	GY-1	2.31 ± 0.09	12.8 ± 0.35	2.00 ± 0.06	20	319 ± 12	3.44 ± 0.15			93 ± 5	Zhuo et al., 2016
NJU-1686	DZ-3	3.01 ± 0.11	12.1 ± 0.33	1.95 ± 0.06	15	167 ± 5	3.54 ± 0.17			47 ± 3	Zhuo et al., 2016
NJU-82	ZZC	2.57	15.2	2.14	13.2	231 ± 4	3.5 ± 0.16	66 ± 4			Wang et al., 2008a,b

loess–paleosol time series (Lu et al., 1999; Ding et al., 2002). The Paleolithic artifact levels of Longgangsi-2 are in the L6, S6, L7, and S7 (MIS 16, 17, 18 and 19) layers (Sun et al., 2017a) with age ranges from ~0.71 Ma to ~0.58 Ma (Lu et al., 1999). The *H. erectus* mandible from Chenjiawo is also in the S6 layer, which was previously dated at ~0.6 Ma (An and Ho, 1989) but is now ~0.67–0.66 Ma based on the new chronology of the Loess Plateau loess–paleosol sequence (Lu et al., 1999). The Bailong Cave site in the Hanjiang River Valley is dated ~0.76 Ma (Liu et al., 2015). All these Paleolithic sites and spots therefore date from ~1.2 Ma to −0.6 Ma (Fig. 4 and Table 3).

The Paleolithic artifact levels of Liuwan in the Luonan Basin are in the tripartite S5 layer (MIS 13, 14, and 15) (Sun et al., 2014) with an age range of ~0.58–0.47 Ma (Lu et al., 1999). All Paleolithic artifact levels of Yaochangwan, and Luojiacun spots in the Hanzhong and Ankang basins are also in the S5 layer (Sun et al., 2012, 2017a) similar to those at Wujiagou and Jiuchang in the Yunxian Basin (Sun et al., in another paper). All these Paleolithic sites and spots therefore date from ~0.6 Ma to 0.5 Ma (Fig. 4 and Table 3).

In the new excavation at Longgangsi-1 in Hanzhong Basin, the Paleolithic artifacts are distributed throughout the loess section from top to bottom. The loess sections at Longgangsi-1 (12 m in depth) and Yaochangwan (15 m in depth) (Sun et al., 2012; Wang and Lu, 2016) are on the same terrace, at a similar altitude, have similar thicknesses, and are only 2.8 km away from one another. Based on their description and comparison in the field, we deduce that they have the same age range. We also deduce that Longgangsi-1 comprise an artifact level that dates from ~0.58 Ma to ~0.07 Ma. Two concentrated Paleolithic artifact levels are at the top part with an age of ~0.1 Ma and at the bottom part with an age range of ~0.58–0.47 Ma.

The Paleolithic artifact level of Longyandong Cave has an age range of ~0.39–0.27 Ma (Sun et al., 2013), which is highly similar to those of the L4 (MIS 10) and S3 (MIS 9) layers. Two Paleolithic artifact levels of Jijiawan are in the S4 and S3 layers (Zhuo et al., 2016). The age of the Dali hominin site near the QMR is ~0.26–0.27 Ma in the L3 layer (MIS 8) (Sun et al., 2017c). All these Paleolithic sites and spots fall within the ~0.43–0.25 Ma stage (Fig. 4 and Table 3).

The following Paleolithic artifact levels date from ~0.20 Ma to ~0.05 Ma: Shizilukou, Zhanghukou, Mengwa, Guoyan, and Zhuangzicun along the South Luohe River (Lu et al., 2007, 2012; Wang et al., 2008a; Wang and Lu, 2016); Hejialiang, Dishuiyan, and Houfang Paleolithic along the Hanjiang River (Sun et al., 2012, 2016; Wang et al., 2014b); and Yangjiaping, Lianfengcun-1, Lianfengcun-2, Liangshancun, Erligou, Shuanghongcun, Chihe, and Qujiahe Paleolithic along the Hanjiang River. Most of these Paleolithic artifact levels are in the S1 (MIS 5), L2 (MIS 6), and S2 (MIS 7) layers. The Huanglong Cave site near the Hanjiang River area is ~0.10–0.08 Ma in the S1 layer (MIS 5) (Shen et al., 2013). All these Paleolithic sites and spots represent the ~0.25–0.05 Ma stage (Fig. 4 and Table 3).

All the Paleolithic artifact levels are within a continuous loess–paleosol sequence from ~1.20 Ma to ~0.05 Ma. Hominin occupation repeatedly occurred in most of the loess (glacial period) and paleosol (interglacial period) layers (Fig. 4 and Table 3). Hominin occurrence is relatively continuous in glacial and interglacial scales. We therefore deduce that hominin occupations of the QMR were almost continuous.

Table 3
Dating ages of Paleolithic sites and spots in the QMR in this paper and previously published paper by our team, and other sites mentioned (*), including Gongwangling, Yunxian, Chenejiawo, Balong Cave, and Huanglong Cave. (Numbering sequences of 40 Paleolithic sites and spots are the same as those in Figs. 2 and 4 and Table 3.)

No.	Site	Age (Ma)	Co-ordinates	Burial position	Reference	Comments
1	Gongwangling*	~1.63 ~1.20 ~1.15	N 34°14′06″, E 109°29′22″		Zhu et al., 2015 Zhu et al., 2003 An and Ho, 1989	Dated by palaeomagnetism; pedostratigraphic correlation with the loess-paleosol sequence
2	Yunxian*	~0.90 ~0.89–0.71	N 32°50′02″, E 110°35′04″		De Lumley and Li, 2008 this paper	Dated by palaeomagnetism; pedostratigraphic correlation with the loess-paleosol sequence
3	Chenjiawo*	~0.71–0.68			An and Ho, 1989	Dated by palaeomagnetism; pedostratigraphic correlation with the loess-paleosol sequence
4	Bailong Cave*	0.76 ± 0.06	N 32°59′40″, E 110°31′34″		Liu et al., 2015	Dated by $^{26}Al/^{10}Be$ burial dating
5	Huanglong Cave*	0.10–0.08	N 33°07′63″, E 110°13′04″		Shen et al., 2013	Dated by U-series dating
6	Longgangsi-3	~1.27–0.71	N 33°04′10.72″, E 106°57′40.70″	on the fifth terrace, ~8 m loess covered	Sun et al., 2017a	Dated by post-IR IRSL; palaeomagnetism; pedostratigraphic correlation with the loess-paleosol sequence
7	Wutaicun	~0.88–0.85	N 32°43′00.21″, E 109°02′07.59″	on the fourth terrace, ~5 m loess covered	Sun et al., 2017a	Dated by post-IR IRSL; palaeomagnetism; pedostratigraphic correlation with the loess-paleosol sequence
8	Shangbaichun	~0.79–0.76	N 34°04′03″, E 110°03′06″	on the second terrace, ~17 m loess covered	Lu et al., 2007	Dated by palaeomagnetism; pedostratigraphic correlation with the loess-paleosol sequence
9	Longgangsi-2	~0.75–0.58	N 33°04′06.96″, E 106°57′50.26″	on the fourth terrace, ~2 m loess covered	Sun et al., 2017a	Dated by post-IR IRSL; palaeomagnetism; pedostratigraphic correlation with the loess-paleosol sequence
10	Yaochangwan	~0.58–0.47	N 33°05′15.86″, E 106°56′46.47″	on the third terrace, ~14 m loess covered	Sun et al., 2012	Dated by TT-OSL; palaeomagnetism; pedostratigraphic correlation with the loess-paleosol sequence
11	Luojiacun	~0.58–0.47	N 32°43′14.37″, E 108°57′52.44″	on the third terrace, ~3.5 m loess covered	Sun et al., 2017a	Dated by post-IR IRSL; palaeomagnetism; pedostratigraphic correlation with the loess-paleosol sequence
12	Liuwan	~0.58–0.47	N 32°59′40″, E 110°31′34″	on the second terrace, ~4.5 m loess covered	Sun et al., 2014; Wang et al., in review	Dated by OSL; $^{26}Al/^{10}Be$ burial dating; palaeomagnetism; pedostratigraphic correlation with the loess-paleosol sequence
13	Qiaojiayao	~0.58–0.47	N 33°59′33″, E 110°59′34″	on the second terrace, ~17 m loess covered	Lu et al., 2011b	Dated by OSL; palaeomagnetism; pedostratigraphic correlation with the loess-paleosol sequence
14	Wujiagou	~0.58–0.47	N 32°49′55.42″, E 110°45′20.58″	on the third terrace, ~5.5 m loess covered	Sun et al., in preparing	Dated by $^{26}Al/^{10}Be$ burial dating; palaeomagnetism; pedostratigraphic correlation with the loess-paleosol sequence
15	Jiuchang	~0.58–0.47	N 32°49′49.89″, E 110°44′26.11″	on the third terrace, ~25 m loess covered	Sun et al., in preparing	Dated by post-IR IRSL; palaeomagnetism; pedostratigraphic correlation with the loess-paleosol sequence
16	Longya Cave	0.39–0.27	N 34°07′37″, E 110°09′34″	on the second terrace	Sun et al., 2013	TT-OSL
17	Jijiawan	0.4–0.1	N 34°16.5′, E 109°10.2′	on the third terrace, ~10 m loess covered	Zhuo et al., 2016	Dated by OSL; post-IR IRSL; palaeomagnetism; pedostratigraphic correlation with the loess-paleosol sequence
18	Dali	0.27–0.26	N 34°52′, E 109°44′	on the third terrace	Sun et al., 2017c	Dated by OSL; TT-OSL; post-IR IRSL
19	Houfang	0.13–0.09	N 32°48′32″, E 110°35′04″			Dated by TT-OSL

(continued on next page)

Table 3 (*continued*)

No.	Site	Age (Ma)	Co-ordinates	Burial position	Reference	Comments
				on the second terrace, ~4 m loess covered	Li et al., 2016a,b Sun et al., 2016	
20	Hejialiang	0.09	N 33°03′52.35″, E 106°57′53.43″	on the second terrace, ~3 m loess covered	Sun et al., 2012	Dated by TT-OSL
21	Dishuiyan	0.11–0.05	N 32°50′07″, E 110°35′32″	on the second terrace, ~3 m loess covered	Sun et al., 2016	Dated by OSL; TT-OSL
22	Shizilukou	0.11–0.05	N 34°05′5.91″, E 110°06′6.27″	on the second terrace, ~2.5 m loess covered	Xing, 2014	Dated by OSL; post-IR IRSL
23	Zhanghuokou	~0.22–0.07		on the third terrace, ~2 m loess covered	Wang and Lu, 2016	Dated by TT-OSL
24	Guoyuan	0.09		on the third terrace, ~3 m loess covered	Wang and Lu, 2016	Dated by TT-OSL
25	Yanling	0.23–0.08		on the third terrace, ~2 m loess covered	Wang and Lu, 2016	Dated by post-IR IRSL
26	Huaishuping	0.09–0.06		on the fourth terrace, ~2 m loess covered	Wang and Lu, 2016	Dated by OSL
27	Zhuangzicun	0.07	N 34°00′46″, E 111°00′37″	on the second terrace, ~5 m loess covered	Wang et al., 2008a,b	Dated by OSL
28	Diaozhai	0.05	N 34°14.1′, E 109°10.2′	on the second terrace, ~6 m loess covered	Zhuo et al., 2016	Dated by OSL; post-IR IRSL
29	Ganyu	0.20–0.10	N 34°14.6′, E 109°10.2′	on the second terrace, ~2 m loess covered	Zhuo et al., 2016	Dated by post-IR IRSL
30	Longgangsi-1	~0.58–0.07	N 33°04′5.41″, E 106°58′07.43″	on the third terrace, ~12 m loess covered	this paper	From sections at the site and at Yanchangwan 2.8 km away
31	Beitaishanmiao	~0.58–0.07	N 32°41′13″, E 110°08′48″	on the third terrace, ~10 m loess covered	this paper	From sections at the site and at Jiuchang ~40 km away
32	Pengjiahe	~0.58–0.07	N 32°39′04″, E 110°14′04″	on the third terrace, ~17 m loess covered	this paper	From sections at the site and at Jiuchang ~45 km away
33	Liangshancun	0.19–0.14	N 33°05′4.04″, E 106°58′05.10″	on the second terrace, ~3.5 m loess covered	this paper	Dated by TT-OSL
34	Chihe	0.15–0.11	N 32°57′34.47″, E 108°19′50.96″	on the second terrace, ~2.4 m loess covered	this paper	Dated by TT-OSL
35	Liangfeng-2	0.17–0.11	N 33°09′11.29″, E 106°45′09.51″	on the second terrace, ~3.5 m loess covered	this paper	Dated by TT-OSL
36	Erligou	0.13–0.11	N 33°12′33.12″, E 107°38′37.06″	on the second terrace, ~4.5 m loess covered	this paper	Dated by TT-OSL
37	Yangjiaping	0.12–0.07	N 33°04′1.01″, E 106°40′28.30″	on the second terrace, ~5.2 m loess covered	this paper	Dated by TT-OSL
38	Liangfeng-1	0.15–0.07	N 33°09′01.44″, E 106°45′09.53″	on the second terrace, ~2 m loess covered	this paper	Dated by TT-OSL
39	Shuanghongcun	0.17–0.11	N 32°57′38.97″, E 108°20′04.66″	on the second terrace, ~1.7 m loess covered	this paper	Dated by TT-OSL
40	Qujiahe	0.13–0.10	N 32°40′59.82″, E 109°03′09.98″	on the third terrace, ~2.8 m loess covered	this paper	Dated by TT-OSL

7. Evaluation of ages for undated Paleolithic artifact levels

7.1. South Luohe River Valley

The records of the Shaanxi Provincial Institute of Archaeology et al. showed that 268 open-air Paleolithic sites were found and described. Most of these sites are on the surface of loess deposits. However, finding and dating each site in situ is extremely difficult. Nonetheless, on the basis of the established chronology of the loess sections and river terrace systems (Lu et al., 2007, 2011a, 2011b, 2012; Wang et al., 2008a; Sun et al., 2013, 2014), we can deduce the ages of these undated Paleolithic sites according to their positions along the South Luohe River terrace. The age of the second terrace is ~0.60 Ma (Lu et al., 2007, 2017; Sun et al., 2014; Wang et al., 2008a) and ~1.10 Ma in the third terrace (Lu et al., 2007, 2011a).

The first terrace comprises Neolithic sites. The Paleolithic artifacts that were collected on the surface of the second and third terraces date from ~0.1 Ma to ~0.20 Ma. In the thick loess sections, on the second terrace, the age range of the Paleolithic artifact level is from ~0.1 Ma to ~0.20 Ma at the top, ~0.3 Ma to ~0.4 Ma in the middle, and from ~0.5 Ma to ~0.6 Ma at the bottom. In the South Luohe River Valley, the age ranges of most sites and spots are ~0.1–0.30 Ma, and only a few of them have age ranges of ~0.5–0.6 Ma.

7.2. Hanjiang River Valley

The sequence data of the Hanjing River terraces in the Hanzhong, Ankang, and Yunxian basins and our dating results for the loess sections on these terraces were used to establish the chronology of the loess–paleosol sequence (Sun et al., 2012, 2016; 2017a, 2017b; Wang et al., 2014a,b; Wang and Lu, 2016). On this basis, we can deduce the age of the undated Paleolithic artifact levels according to their positions in these loess sections. The ages of the terraces are sequenced from low to high (Sun et al., 2016, 2017a), i.e., the second terrace is ~0.20 Ma, the third terrace is ~0.60 Ma, the fourth terrace is ~0.70–0.90 Ma, and the fifth terrace is ~0.80–1.20 Ma.

Similar to those in the South Luohe River Valley, only Neolithic sites were found on the first terrace. On the second terrace, the age range of the Paleolithic artifact level is from ~0.05 Ma to ~0.2 Ma. In the loess sections on the third terrace with thicknesses of ~20 m,

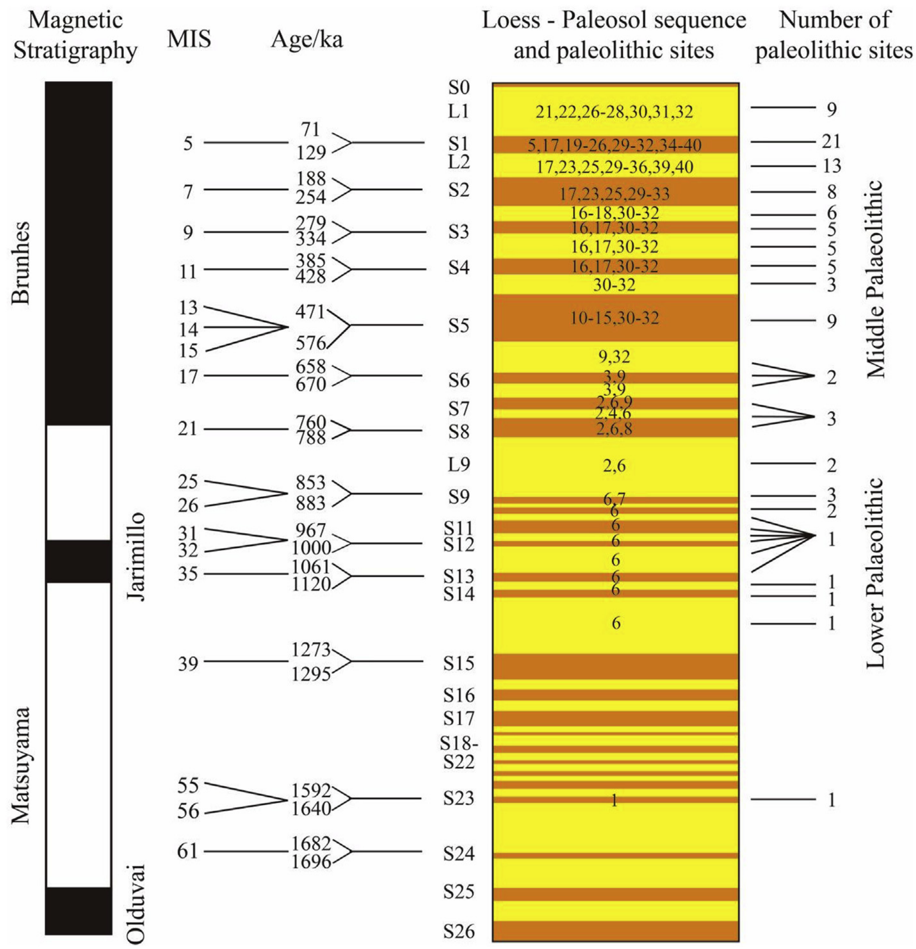

Fig. 4. Polarity, marine isotope stages (MIS), ages, loess–paleosol sequence (Lu et al., 1999; Ding et al., 2002), Paleolithic sites and spots, and number of Paleolithic sites and spots in each loess or paleosol layer. (Numbering sequences of 40 Paleolithic sites and spots are the same as those in Figs. 2 and 4 and Table 3.)

the age ranges of the Paleolithic artifact level are from ~0.1 Ma to ~0.2 Ma on the top, ~0.3 Ma to ~0.4 Ma in the middle, and ~0.5 Ma to ~0.6 Ma on the bottom. On the fourth terrace, the age ranges of the Paleolithic artifact level in the upper part are from ~0.1 Ma to ~0.6 Ma and from ~0.7 Ma to ~0.9 Ma on the lower part of loess sections. On the fifth terrace, the age ranges of the Paleolithic artifact level in loess sections is from ~0.1 Ma to ~0.7 Ma in the upper part and from ~0.9 Ma to ~1.2 Ma in the lower part.

Several Paleolithic sites and spots were excavated and found in the Danjiangkou area (Li et al., 2009, 2012; Pei et al., 2008; Zhou et al., 2009), and they are located only ~70 km away from the Yunxian Basin. Owing to the construction of the Danjiangkou reservoir, all excavated Paleolithic sites on the second and third terraces are now below the current water level. We have previously consolidated the dating result of the Hanjiang River terrace in the Yunxian Basin. On this basis, attempts were made to evaluate the ages of these undated Paleolithic sites below water.

Only a few loess sections, such as those at Beitaishanmiao (~12 m) and Pengjiahe (~30 m) sites on the third terrace, are from ~0.1 Ma to ~0.6 Ma. Most Paleolithic sites and spots, such as Waibianguo, Datubao, Guochachang, Songwan, and Hangjiawanin, that are covered by thin loess sections on the second or third terraces may date from ~0.1 Ma to ~0.30 Ma. All Paleolithic artifacts collected from the surfaces of the second, third, and fourth terraces may date from ~0.1 Ma to ~0.30 Ma.

8. Paleolithic industry

The QMR Paleolithic assemblages can be divided into early, middle, and late stages based on their positions within the loess–paleosol sections. All lithic artifacts contained local pebbles/cobbles from the nearby riverbank. The earliest QMR Paleolithic assemblage identified thus far is from the Longgangsi-3 site (Fig. 5, a1–a10) and dated between ~1.2 Ma and ~0.7 Ma (Fig. 6). The raw material is mainly vein quartz. The utilized principal flake knapping method involved the use of a direct hammer hard percussion with some bipolar techniques. Most lithic artifacts are small (<50 mm). Retouched tools included light-duty scrapers. With regard to the retouched tools, most removal positions are direct and inverse.

The middle QMR Paleolithic industry is represented by Liuwan, Qiaojiayao, and the Longyadong Cave (Shaanxi Provincial Institute of Archaeology, 2008) (Fig. 5, b1–b11), and they are dated from ~0.6 to ~0.3 Ma. The raw material is mainly vein quartz and quartzite. The utilized principal flake knapping method involved the use of the direct hammer hard percussion. Both small- and large-sized artifacts were observed. Most removal positions of retouched tools are direct and inverse. The lithic artifacts comprised hammer stones, cores, flakes, retouched tools, and


a1
a2
a3
a4
a5
a6
a7
a8
a9
a10
b1
b2
b3
b4
b5
b6
b7
b8
b9
b10
b11
c1
c2
c3
c4
c5
c6
c7
c8
c9

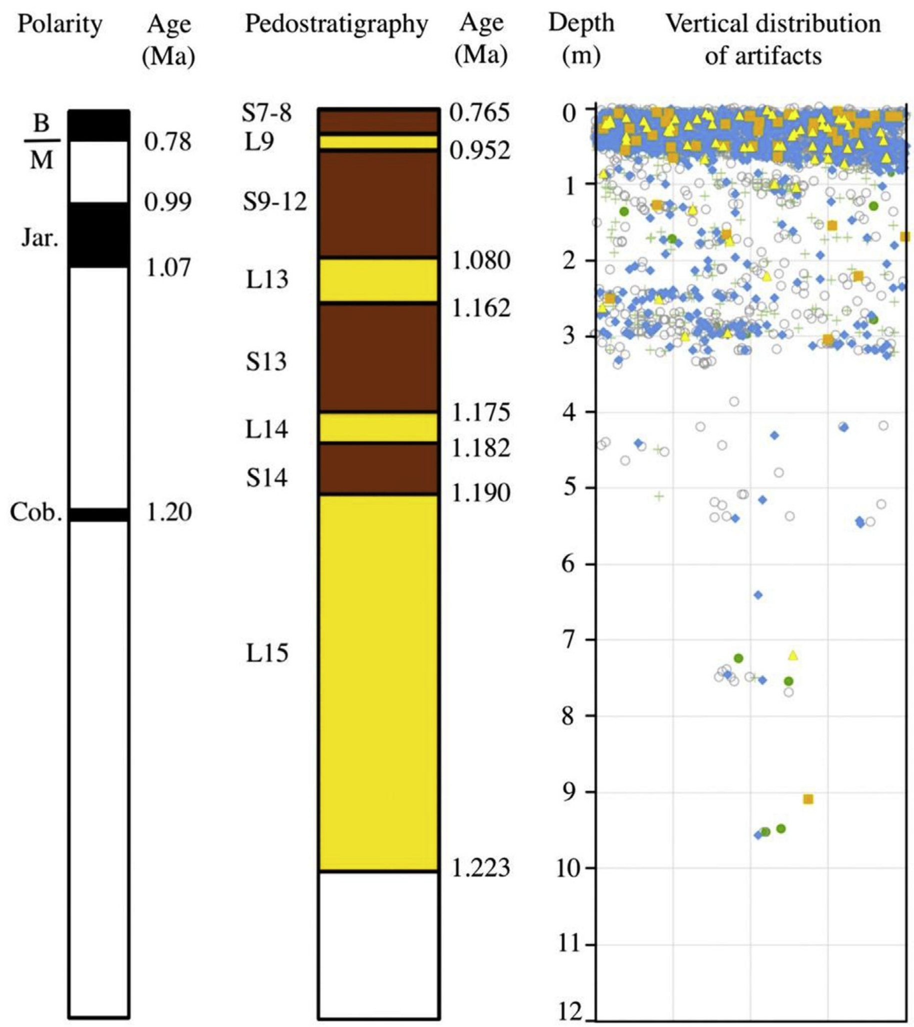

Fig. 6. Polarity, pedostratigraphy, depth, and vertical distribution of lithic artifacts excavated from Longgangsi-3 site. Note the presence of artifacts in L9, L13, L14, and L15.

flaking debris. The early and middle QMR Paleolithic industries belong to Mode 1. In this paper, we refer to "Chinese Mode 1" when referring to a type of old Paleolithic industry; however, the classification is not a rule of age judgment, as Chinese Mode 1 clearly occurred in the early, middle, and very late Pleistocene.

The most recent QMR Paleolithic assemblages are represented by the Hejialiang, Dishuiyan, and Houfang sites, and artifact collections were conducted in more than 200 sites and spots (Shaanxi Provincial Institute of Archaeology, 2007) (Fig. 5, c1–c9). The age range is from ~0.3 to ~0.05 Ma. The raw material is mainly vein quartz, quartzite, and limestone pebbles/cobbles. The lithic artifacts contain hammer stones, cores, flakes, retouched tools, and flaking debris. Spheroidal and Acheulian-type large cutting tools (LCTs), such as hand axes (Fig. 3), picks, and cleavers, are also present. The late QMR Paleolithic industry belong to Mode 2. The age of the hand axes in the QMR is from ~0.3 Ma to ~0.05 Ma.

The discovery of Acheulean-type tools in China has been a source of debate for many years. Hand axes have been discovered in several localities, such as Bose, Dingcun, Luonan, and Danjiangkou. Researchers generally believe that LCTs can be found in the Luonan Basin, in which hand axes, picks, and cleavers are the most typical. Luonan and Danjiangkou belong to the QMR. On the basis of our investigations and dating results, all Acheulean-type tools in Dingcun, Luonan, and Danjiangkou localities can be associated with the late Pleistocene.

9. Glacial–interglacial environmental changes and hominin evolution in the QMR

9.1. Glacial–interglacial environmental records in the central CLP

The classic Luochuan loess–paleosol sequence on the central Loess Plateau depicts a continuous record of paleo–environmental changes dominated by winter and summer monsoons during the glacial and interglacial periods (e.g., Liu, 1985; Kukla and An, 1989; An et al., 1990; Lu et al., 1999, 2010; An, 2000; Guo et al., 2002). The magnetic susceptibility stratigraphy of the Luochuan loess–paleosol sequence is highly correlated with the marine oxygen isotope record (e.g., Heller and Liu, 1984).

The marine oxygen isotope and magnetic susceptibility stratigraphy of the loess–paleosol sequence record of the central CLP indicates that global ice volume dynamics underwent a

Fig. 5. Representative early Paleolithic artifacts from Longgangsi-3 site (a1–a10), middle Paleolithic artifacts from Liuwan (b1–b6), and Longya Cave (b7–b11) in the QMR and late Paleolithic artifacts from Luonan Basin (c1–c9) in the QMR.

fundamental change during the mid-Pleistocene transition (MPT) between 1.25 Ma and 0.7 Ma (Shackleton et al., 1995; Lu et al., 2010) (Fig. 7B). During the MPT, the dominant periodicity of the climatic cycles (cyclicity) changed from 41 kyr to 100 kyr; by contrast, after the MPT, the climatic cycles were predominantly 100 kyr (Lu et al., 2004) (Fig. 7B).

On the basis of the susceptibility stratigraphy of the Luochuan loess section, the climate changes in the Loess Plateau beginning ~1.2 Ma shifted to high aridity, hence the marked contrasts between glacial and interglacial scales (Fig. 7B). During the MPT between 1.2 Ma and 0.7 Ma, two cold and dry glacials occurred at 0.79–0.85 Ma and 1.265–1.273 Ma, respectively (Lu et al., 1999) (Fig. 7C; blue stage). During the stage after ~0.60 Ma, the contrasts between glacial and interglacial scales are the greatest, and longer and warmer humid interglacial environments were dominant (Fig. 7C; red stage).

Luochuan is located only ~150 km away from the QMR (Fig. 1). At present, the average annual temperature of Luochuan is ~2°–4° lower and the average annual rainfall is ~200–400 mm lower than those in the QMR. The climates of the Loess Plateau and QMR are controlled by EAM. Therefore, the environmental changes recorded for the glacial and interglacial scales in Luochuan are coincident with those in the QMR (i.e., small differences in temperature and rainfall).

9.2. Environmental changes and hominin evolution in the QMR

According to the most recent reports, the earliest evidence of hominins in Asia is in the Shangchen site in Lantian in the northern Qinling Mountains with, and the age range is 2.12–1.26 Ma (Zhu et al., 2018).

The first appearance of lithic artifacts in the southern Qinling Mountains is in the L15 layer (MIS 38) (ca. 1.26–1.21 Ma) at Longgangsi-3, which can represent the start of MPT. The climatic condition corresponding to the deposition of the L15 layer (a particularly thick and silty layer) was extremely severe, and the estimated annual average temperatures on the Loess Plateau could have been as low as 1.5 °C–3.0 °C with rainfall of only 150–250 mm p. a. (Guo et al., 1998). During the deposition of L15, the Loess Plateau was highly likely depopulated and the southern QMR was a glacial refugium. In addition, the L9 layer is a thick and silty unit and was deposited in a cold arid climate. Given that the QMR was occupied during these extremely cold periods, it was likely a refugium with an age range of ~1.2 Ma and ~0.85 Ma (i.e., northern China was not a place for permanent year-round settlement for hominins during the longer and more severe glacial periods) (Dennell, 2013). On the basis of the distribution of lithic artifacts in the loess section profile of Longgangsi-3, it is probable that the

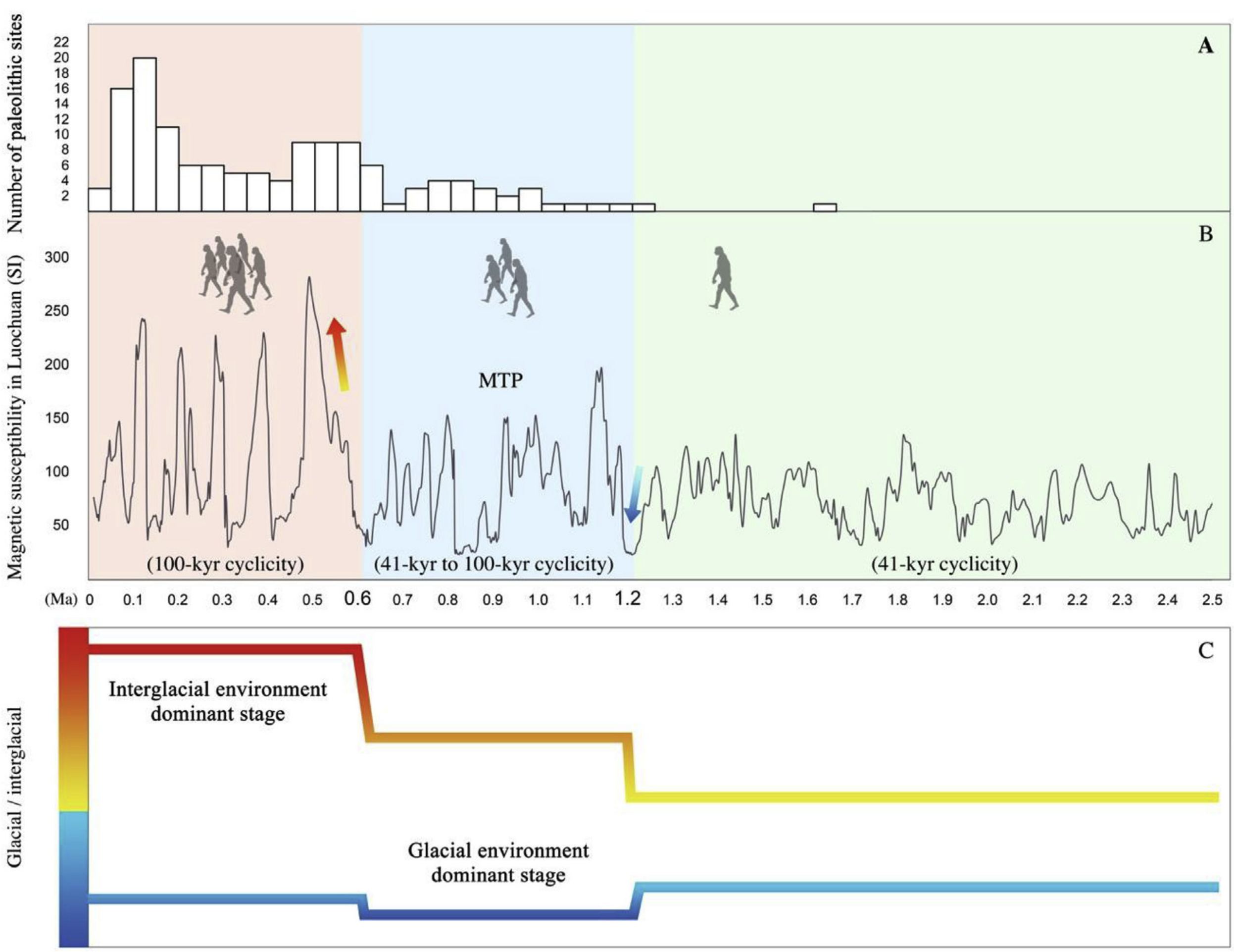

Fig. 7. Environmental changes and hominin settlement in the QMR. A: Number of Paleolithic sites and spots from ~1.2 Ma to ~0.05 Ma. B: Magnetic susceptibility record of the Luochuan loess section (Lu et al., 1999) showing the large drying events and large humid and warm events. C: Glacial environment dominant stage (mid-Pleistocene transition; MPT) (blue) and interglacial environment dominant stage (red). (For interpretation of the references to color in this figure legend, the reader is referred to the Web version of this article.)

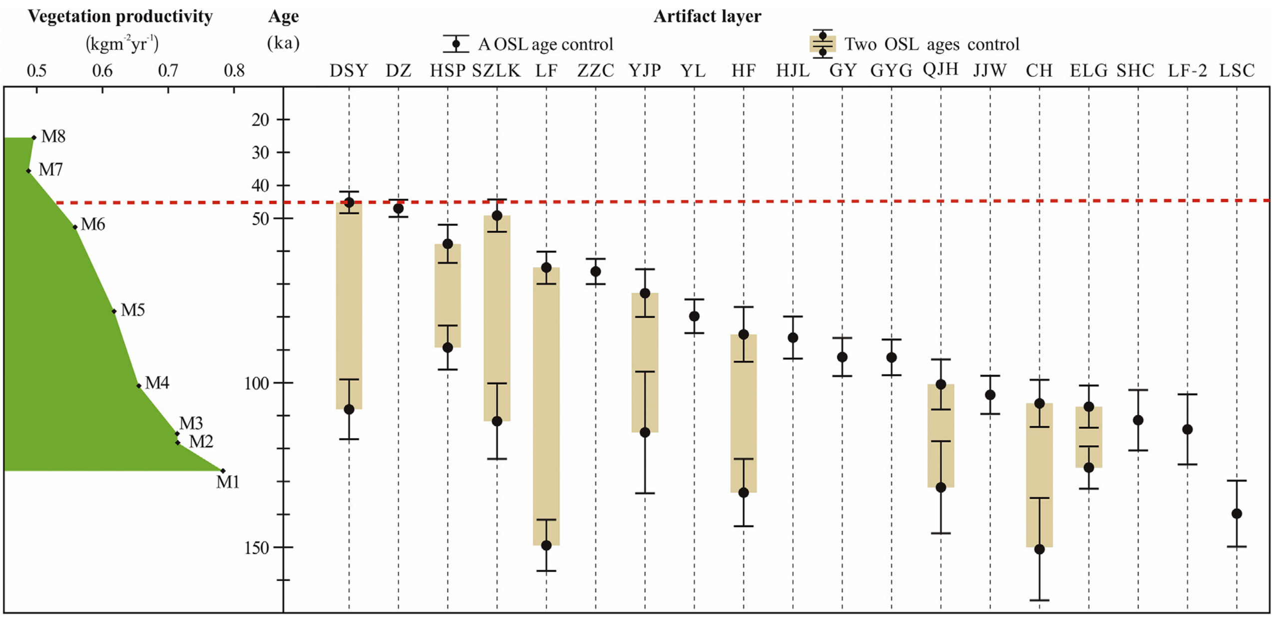

Fig. 8. Decline in human occupation (i.e., decrease in GPP) beginning ~0.05 Ma (red dotted line). (For interpretation of the references to color in this figure legend, the reader is referred to the Web version of this article.)

hominin settlement in the QMR was continuous (i.e., from L15 (MIS 38) to S7 (MIS 19) layers with age range between ~1.2 Ma and ~0.7 Ma) because hominins existed in both glacial and interglacial periods (Fig. 7A).

Considerable evidence has proven the hominin occupation of the QMR between ~0.6 Ma and ~0.05 Ma. The long humid and warm event represented by the tri-partite S5 layer (= MIS 13, 14, 15) after the long glacial period (L6; = MIS16) could have provided the optimal environment for hominin settlement and dispersal (Fig. 7A). In the Loess Plateau, the greatest Middle Pleistocene warmth was recorded to be in paleosols, i.e., S4 (385–428 ka, = MIS 11), S5-1 (471–510 ka, = MIS 13), and S5–3 (560–576 ka = MIS 15) (Lu et al., 1999). These paleosols were formed under sub-tropical semi-humid climates with tentatively estimated mean annual temperature of 2 °C–6.8 °C (higher than present) and mean annual precipitation of 200–300 mm (higher than present), which indicate a much strengthened summer monsoon (Guo et al., 1998). The Last Interglacial period at ca. 129–71 ka is the second optimal period for hominins (Fig. 7A), and it offers the most apparent evidence of hominin activity in the QMR.

Nearly 400 Paleolithic artifact sites and spots, several of which have been excavated, with age range of ~0.6–0.05 Ma render the QMR an important area of hominin settlement during the Middle and Late Pleistocene. During this stage, many hominin occupations and activities have been recorded for the interglacial periods, as opposed to the few records in the same scenarios for the glacial periods. This finding is important because it suggests the occurrence of both cold and warm periods; moreover, during the cold periods, the QMR provided the circumstance for the source populations to re-colonize northern China where conditions had improved (Figs. 4 and 7).

10. What caused a drastic decrease in human occupation of the QMR beginning ~50 ka?

Hominin occupation and settlement in the QMR were concentrated during the late Pleistocene, especially at ~0.1 Ma. However, based on our dating results (Fig. 8 and Table 2), hominin occupation and settlement decreased substantially after ~50 ka (Fig. 8). A direct

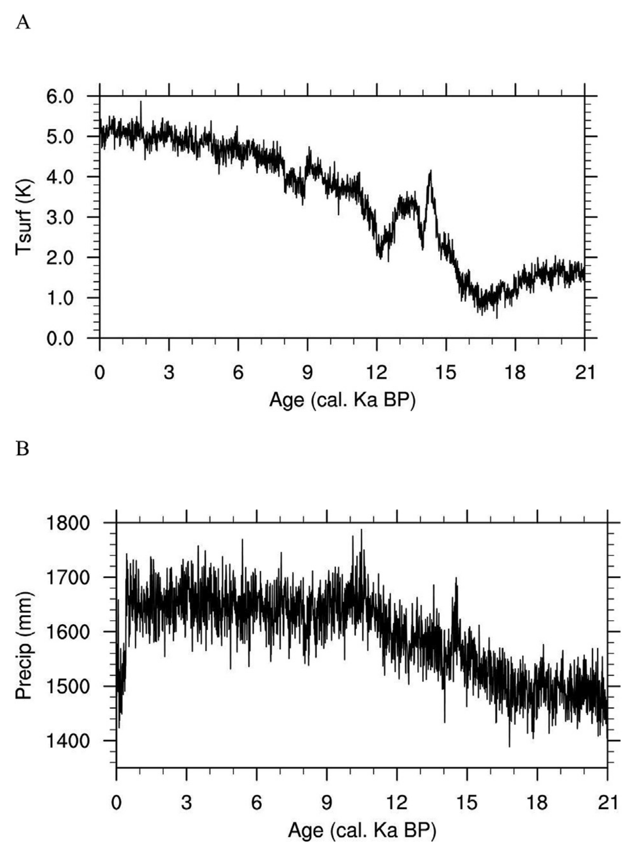

Fig. 9. A: TraCE-21ka for the QMR by using DOE INCITE with temperature changes since the last glacial maximum (MIS 2).
B: TraCE-21ka for the QMR by using DOE INCITE with moisture changes since the last glacial maximum (MIS 2).

Table 4A
Simple alternations of EAM are supposed to be coupled with continental ice volume (ideal scenario). We obtained the inferential ages and temperature change of the QMR from the Last Interglacial (130 ka) to the last glacial (25 ka) periods.

Age range 0–25.8 ka	Temperature difference (°C) in Antarctica	Temperature difference (°C) in QMR	Carbon dioxide (ppm.)	Age range 25.8–127.6 ka	Temperature difference (°C) in Antarctica	Temperature difference (°C) in QMR	Carbon dioxide (ppm.)
–	–	–	–	126.0–127.6	+2	+1	268
Current	0	0	280	117.5–119.0	0	0	270
11.8–12.0	−2	−1	246	115.0–116.0	−2	−1	268
13.0–14.3	−4	−2	237	100.4–101.5	−4	−2	234
15.5–16.3	−6	−3	214	52.2–53.2	−6	−3	190
16.6–17.1	−8	−4	197	35.2–36.0	−8	−4	205
25.2–25.8	−10	−5	192	25.2–25.8	−10	−5	192

Table 4B
Settings of eight stages (M1–M8) based on a simulated scenario: 1 °C (temperature), concentration of two oxygen carbon, and precipitation of the QMR.

Setting	Temperature difference (°C)	Carbon dioxide (ppm.)	Precipitation (mm)	Age range 128-25ka
Current	0	378	800–1000	0
M1	+1	268	>1000	126.0–127.6
M2	0	270	800–1000	117.5–119.0
M3	−1	268	800–1000	115.0–116.0
M4	−2	234	800–1000	100.4–101.5
M5	−3	219	800–1000	77.7–79.0
M6	−3	190	800–1000	52.2–53.2
M7	−4	205	<800	35.2–36.0
M8	−5	192	<800	25.2–25.8

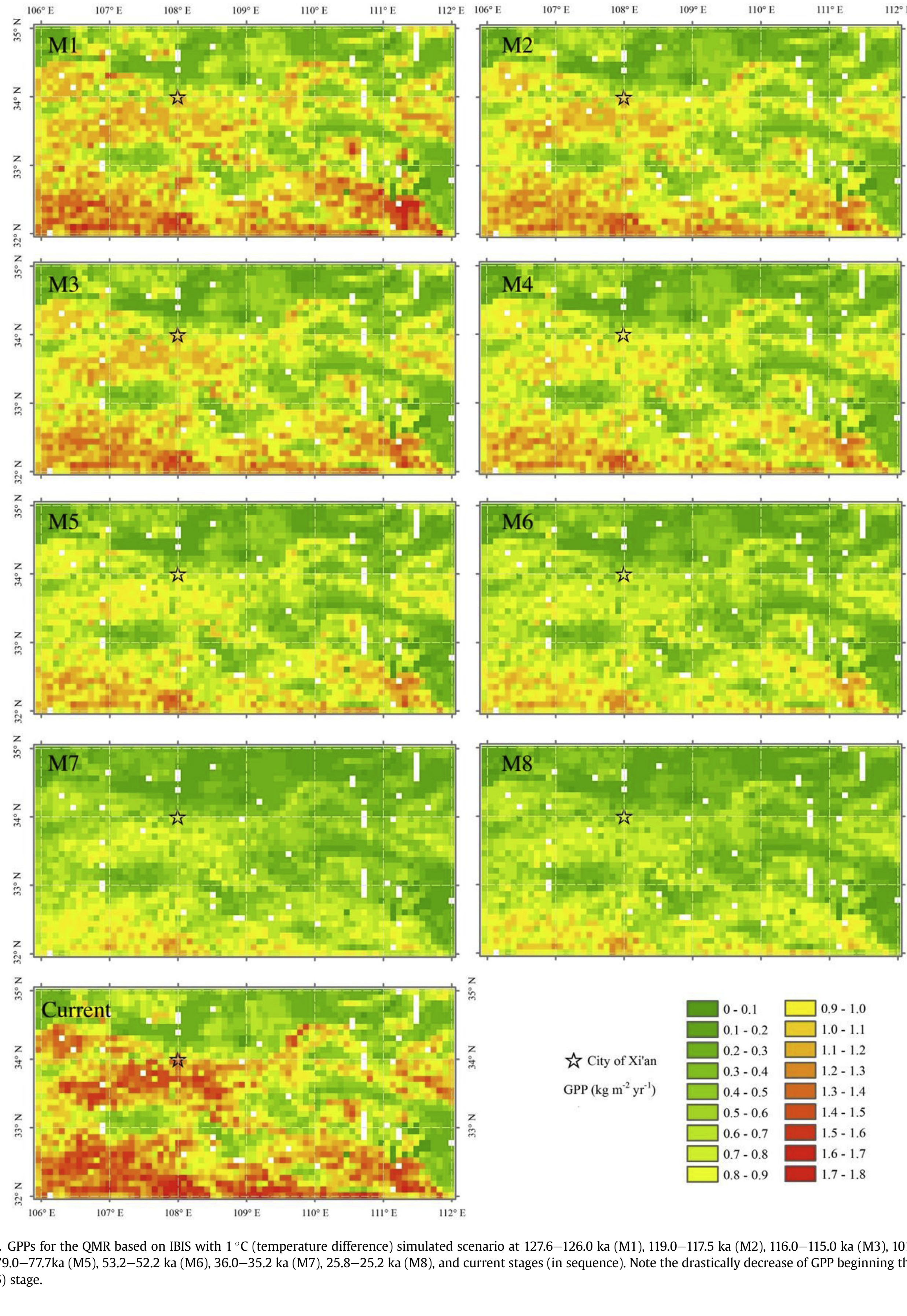

Fig. 10. GPPs for the QMR based on IBIS with 1 °C (temperature difference) simulated scenario at 127.6–126.0 ka (M1), 119.0–117.5 ka (M2), 116.0–115.0 ka (M3), 101.5–100.4 ka (M4), 79.0–77.7ka (M5), 53.2–52.2 ka (M6), 36.0–35.2 ka (M7), 25.8–25.2 ka (M8), and current stages (in sequence). Note the drastically decrease of GPP beginning the 53.2–52.2 ka (M6) stage.

Table 5
Changes of GPP based on different vegetation types for M1–M8 stages (units: $kg\cdot m^{-2}\,yr^{-1}$) versus current stage (i.e., 2000–2009).

vegtype	current	S1	S2	S3	s4	S5	S6	S7	S8
TEBF	1.394799	1.326351	1.254846	1.266697	1.211554	1.177152	1.102119	1.025327	1.048562
TECF	1.203099	1.050324	1.010642	1.011682	0.917486	0.865063	0.767977	0.765073	0.727182
BEF	0.760915	0.600859	0.601469	0.577909	0.488698	0.436406	0.373564	0.387232	0.339995
Sav.	0.977285	1.0187	0.922	0.902995	0.860969	0.814848	0.772384	0.678847	0.687487
Ste.	0.534712	0.579117	0.526826	0.505047	0.47368	0.446537	0.432404	0.383412	0.381981
Den.Shr.	0.346866	0.365848	0.35666	0.351901	0.347289	0.34587	0.348677	0.334807	0.337385
Op.Shr.	0.147319	0.153594	0.150585	0.149898	0.142049	0.137542	0.126149	0.116631	0.116711
mean	0.834573	0.783246	0.714446	0.713631	0.6553	0.617644	0.558162	0.487484	0.495836

TEBF: temperate evergreen broadleaf forest/woodland; TECF: temperate evergreen conifer forest/woodland; BEF: boreal evergreen forest/woodland; Sav.: savanna; Gra.: grassland/steppe; Den.Shr.: dense shrubland; Op.Shr.: open shrubland. (No changes made to vegetation types: tropical evergreen forest/woodland; tropical deciduous forest/woodland; temperate deciduous forest/woodland; boreal deciduous forest/woodland; mixed forest/woodland; tundra; desert; polar desert/rock/ice.)

factor considered in this study is climate change.

10.1. Climate change setting

Climate change, an integrated process involving temperature, moisture, and vegetation factors, has been reconstructed in a number of global and/or regional paleoclimate records. Temperature, CO_2, and moisture changes may not directly shape human activities, but ecological structures and resource alterations are factors that can directly shape human evolution. The links in these relationships have been established as follows: climate change → temperature, CO_2, and moisture → ecological structure and resource change → human response and adaptation. The arrows represent successive relation.

EAM is an important component of the global climate system, and it has exerted major control of the climate changes in East Asia (An, 2000). Characterized by long-term alternations, the EAM in this region is also coupled with continental ice volume (Ding et al., 2002; Lu et al., 2004, 2010). The QMR is a natural barrier between the southern and northern climatic regimes of China, which is controlled by EAM (Lu et al., 2002, 2012; Zhang et al., 2012). Although the records on climate change (e.g., temperature and moisture) have been reconstructed for many sites in global and/or regional research, the climatic reconstructions in the QMR are rare. The few studies that employed pollen analyses for central China have estimated the range of temperature change to be approximately 5 °C since the last glacial period (Zheng et al., 2016).

TraCE-21ka (Liu et al., 2009, 2014) was used to reconstruct temperature and moisture since the last glacial maximum (MIS 2) in the QMR was derived by using the DOE INCITE computing program. The findings show that the change in temperature was ca. 5 °C (Fig. 9A) while the moisture change was ca. 200 mm between the glacial and interglacial periods (Fig. 9B).

EAM is coupled with continental ice volume (Ding et al., 2002; Lu et al., 2004, 2010). Thus, the TraCE-21ka climate simulation data and the pollen analytical results were used as basis for establishing the correlation of age, temperature change, and CO_2 in the QMR from the Last Interglacial period (130 ka) to the last glacial period (25 ka) (Table 4A). Our analysis showed that the temperature of the QMR from the Last Interglacial (130 ka) to the last glacial period (25 ka) decreased by 6 °C, and the precipitation was reduced by ~200 mm (Table 4B).

10.2. Vegetation productivity

We propose a new method to express ecological structure and change of resource availability, particularly by using the change of vegetation productivity, after the climate change during the last glacial and interglacial cycles. Then, we determined the relationship between climate change and vegetation productivity change. Vegetation productivity is the overall rate of photosynthesis or chemosynthesis. In ecosystems, vegetation productivity represents the ability of an ecosystem to absorb CO_2 from the atmosphere. It is sensitive to changes of environmental factors, such as precipitation, temperature, and CO_2 concentration.

Gross primary productivity (GPP), or the overall rate of biomass production by photosynthesis, was used to represent vegetation productivity. In this study, GPP was simulated by the Integrated Biosphere Simulator (IBIS) (Foley et al., 1996; Farquhar et al., 1980; Liu et al., 2005). IBIS can compare observations in regional and global scales according to several studies (Kucharik et al., 2000; Lu et al., 2016). As a dynamic global vegetation model, IBIS can perform historical and future simulations of Intergovernmental Panel on Climatic Change (IPCC) scenarios for land process modeling (Cramer et al., 2001).

Given the type of data, particularly for climatic reconstruction (Table 4), dynamic IBIS modeling was performed to simulate a 1 °C temperature scenario. Then, we further simulated the changes of GPP for the Qinling Mountains. The results showed that at 127.6–126.0, 119.0–117.5, 116.0–115.0, 101.5–100.4, 79.0–77.7, 53.2–52.2, 36.0–35.2, and 25.8–25.2 ka (M1–M8 stages, in sequence), the mean GPP in the QMR changed by 0.78 (M1), 0.71 (M2), 0.71 (M3), 0.66 (M4), 0.62 (M5), 0.56 (M6), 0.49 (M7), 0.50 (M8), and 0.83 (current) kg $m^{-2}\,yr^{-1}$ (in sequence) (Figs. 8 and 10; Table 5).

10.3. Human activity decreased drastically with GPP plunge

Between 127.6 ka and 25.2 ka in the QMR, a marked plunge in GPP was derived for the M6 stage (0.56 kg $m^{-2}\,yr^{-1}$) starting at 53.2 ka (Figs. 8 and 10). The minimum GPP value is ca. 36.0–35.2 ka in the M7 stage. The decline in value and the minimum value of GPP are synchronous with the data depicting the evidential decrease in human activity beginning the M6 stage (53.2–52.2 ka) (Figs. 8 and 10).

11. Conclusions

On the basis of OSL, TT-OSL, post-IR IRSL, paleomagnetic, and $^{26}Al/^{10}Be$ burial dating of the 35 Paleolithic sites and the spots discovered by our team, we established the age sequence (from ~1.20 Ma to ~0.05 Ma) for hominin occupation in the QMR in central China. The finding of the earliest lithic artifacts in the southern Qinling Mountains is in the L15 layer (MIS 38) (ca. 1.27–1.21 Ma) at Longgangsi-3. Hominin occupation and settlement likely expanded from ca. 0.58 Ma to 0.47 Ma (S5; MIS 13, 14, 15) and from ca. 0.13 Ma to 0.07 Ma (S1; MIS 5). However, Hominin occupation drastically decreased after ~0.05 Ma.

We also investigated how hominin groups responded to

glacial–interglacial shifts from ~1.20 Ma to ~0.05 Ma in the QMR. The longer and more severe cold and dry climatic events after ~1.2 Ma may have forced hominins to retreat from northern China to the QMR, where it was possible to live in both cold and warm periods. The optimal periods for settlement accord with the deposition of the tri-partite S5 layer (MIS 13, 14, 15) (ca. 0.58–0.47 Ma) and S1 layer (MIS 5) (ca. 0.13–0.07 Ma) of the interglacial period. More hominin occupations during ~0.6–0.05 Ma were recorded for the interglacial periods than for the glacial periods.

The hominin occupations were relatively continuous during the glacial and interglacial periods. The QMR was likely a source area for continuous hominin settlement in central China, part of the migration route for hominins between northern and southern China, and a refugium during the cold periods. The drastic decline of human occupation of the QMR after ~0.05 Ma can be linked to the decline in GPP, which was driven by climate change.

Acknowledgments

We thank Xiaobo Feng, Yinghua Li, Haixin Zhuo, and Kaifeng Yu for helping in the field excavations. This research is supported by the National Natural Science Foundation of China (Grant Nos. 41572155, 41472026, and 41690111), the Global Change Program of the Ministry of Science and Technology of China (Grant No. 2016YFA0600503), and the CAS Strategic Priority Research Program Grant B (XDPB05).

References

An, Z.S., Ho, C.K., 1989. New magnetostratigraphic dates of Lantian Homo erectus. Quat. Res. 32, 213–221.
An, Z.S., Liu, T.S., Lu, Y.C., Porter, S.C., Kukla, G., Wu, X.H., Hua, Y.M., 1990. The long-term palaeomonsoon variation recorded by the loess-paleosol sequence in central China. Quat. Int. 7, 91–95.
An, Z.S., 2000. The history and variability of the East Asian paleomonsoon climate. Quat. Sci. Rev. 19, 171–187.
Bahain, J.-J., Shao, Q.F., Han, F., Sun, X.F., Voinchet, P., Liu, C.R., Yin, G.M., Flagueres, C., 2017. Contribution of ESR et ESR/U-series methods to the dating of some Pleistocene sites of Chin. Anthropologie 121, 215–233 (in France with English abstract).
Buylaert, J.P., Vandenberghe, D., Murray, A.S., Huot, S., Corte, F.D., Van de Haute, P., 2007. Luminescence dating of old (>70 ka) Chinese loess: a comparison of single-aliquot OSL and IRSL techniques. Quat. Geochronol. 5, 9–14.
Buylaert, J.P., Jain, M., Murray, A.S., Thomsen, K.J., Thiel, C., Sohbati, R., 2012. A robust feldspar luminescence dating method for Middle and Late Pleistocene sediments. Boreas 41, 435–451.
Cramer, W., Bondeau, A., Woodward, F.I., Prentice, I.C., Betts, R.A., Brovkin, V., Cox, P.M., Fisher, V., Foley, J.A., Friend, A.D., Kucharik, C., Lomas, M.R., Ramankutty, N., Sitch, S., Smith, B., White, A., Young-Molling, C., 2001. Global response of terrestrial ecosystem structure and function to CO_2 and climate change: results from six dynamic global vegetation models. Global Change Biol. 7, 357–373.
De Lumley, H., Li, T., 2008. Le site de l'Homme de Yunxian: Quyuanhekou, Quingqu, Yunxian, Province Du Hubei. CNRS, Paris.
Dennell, R.W., 2013. The Nihewan Basin of north China in the early pleistocene: continuous and flourishing, or discontinuous, infrequent and ephemeral occupation. Quat. Int. 295, 223–236.
Deng, C.L., Zhu, R.X., Zhang, R., Ao, H., Pan, Y.X., 2008. Timing of the Nihewan formation and faunas. Quat. Res. 69, 77–90.
Ding, Z.L., Derbyshire, E., Yang, S.L., Yu, Z.W., Xiong, S.F., Liu, T.S., 2002. Stacked 2.6 Ma grain size from the Chinese loess based on five sections and correlation with the deep-sea $\delta^{18}O$ record. Paleoceanography 17, 5-1-5-21.
Du, S.S., Liu, F.L., Zhu, S.W., Zhang, M., 2008. Loess paleoliths from Lushi county, henan province. Quat. Sci. 28, 1000–1006 (in Chinese with English abstract).
Farquhar, G.D., von Caemmerer, S., Berry, J.A., 1980. A biochemical model of photosynthetic CO_2 assimilation in leaves of C_3 species. Planta 149, 78–90.
Foley, J.A., Prentice, I.C., Ramankutty, N., Levis, S., Pollard, D., Sitch, S., Haxeltine, A., 1996. An integrated biosphere model of land surface processes, terrestrial carbon balance, and vegetation dynamics. Global Biogeochem. Cycles 10, 603–628.
Gao, X., 1999. A discussion on "Chinese middle Paleolithic". Acta Anthropol. Sin. 18, 1–16.
Gao, X., Hou, Y.M., 2002. Paleolithic Archaeology in the Twentieth Century. Cultural Relics Press, Beijing (in Chinese).
Gao, X., Yuan, B.Y., Pei, S.W., Wang, H.M., Chen, F.Y., Feng, X.W., 2008. Analysis of sedimentary-geomorphologic variation and the living environment of hominids at the Shuidonggou Paleolithic site. Chin. Sci. Bull. 53, 2025–2032.
Gao, X., 2013. Paleolithic cultures in China uniqueness and divergence. Curr. Anthropol. 54, 358–370.
Guo, Z.T., Liu, T.S., Fedoroff, N., Wei, L.Y., Ding, Z.L., Wu, N.Q., Lü, H.Y., Jiang, W.Y., An, Z.S., 1998. Climate extremes in loess in China coupled with the strength of deep-water formation in the North Atlantic. Global Planet. Change 18, 113–128.
Guo, Z.T., Ruddiman, W.F., Hao, Q.Z., Wu, H.B., Qiao, Y.S., Zhu, R.X., Peng, S.Z., Wei, J.J., Yuan, B.Y., Liu, T.S., 2002. Onset of Asian descertification by 22 Myr ago inferred from loess deposits in China. Nature 6877, 159–163.
Heller, F., Liu, T., 1984. Magnetism of Chinese loess deposits. Geophys. J. Roy. Astron. Soc. 77, 125–141 s.
Hou, Y.M., Potts, R., Yuan, B.Y., Guo, Z.T., Deino, A., Wang, W., Clark, J., Xie, G.M., Huang, W.W., 2000. Mid-Pleistocene Acheulean-like stone technology of the Bose basin, south China. Science 287, 1622–1626.
Huang, W.W., 2000. Stratigraphical basic of the paleolithic sequence of China. Acta Anthropol. Sin. 19, 269–283 (in Chinese with English abstract).
Ji, D.X., Chen, F.H., Bettinger, R.L., Elston, R.G., Geng, Z.Q., Barton, L., Wang, H., An, C.B., Zhang, D.J., 2005. Human response to the last glacial maximum: evidence from north China. Acta Anthropol. Sin. 25, 270–282 (in Chinese with English abstract).
Kucharik, C.J., Foley, J.A., Delire, C., Fisher, V.A., Coe, M.T., Lenters, J.D., Young-Molling, C., Ramankutty, N., Norman, J.M., Gower, S.T., 2000. Testing the performance of a dynamic global ecosystem model: water balance, carbon balance, and vegetation structure. Global Biogeochem. Cycles 14, 795–825.
Kukla, G., An, Z.S., 1989. Loess stratigraphy in Central China. Palaeogeogr. Palaeoclimatol. Palaeoecol. 72, 203–225.
Li, B., Li, S.H., 2011. Luminescence dating of k-feldspar from sediments: a protocol without anomalous fading correction. Quat. Geochronol. 6, 468–479.
Li, C.R., Feng, X.W., Li, H., 2009. A study of the stone artifacts discovered in the Danjiangkou reservoir area in 1994. Acta Anthropol. Sin. 28, 337–354 (in Chinese with English abstract).
Li, F., Chen, F.Y., Wang, Y.H., Gao, X., 2016a. Technology diffusion and population migration reflected in blade techniques in northern China in the late pleistocene. Sci. China Earth Sci. 59, 1540–1553.
Li, H., Li, C.R., Feng, X.W., 2012. A study on the stone artifacts from 2004 field investigation in Danjiangkou reservoir area, Hubei and Henan, China. Acta Anthropol. Sin. 31, 113–126 (in Chinese with English abstract).
Li, X.Q., Gao, Q., Hou, Y.M., Zhao, K.L., Sun, N., Yang, Z.M., Zhen, Z., Liu, Y., Zhou, X.Y., 2014a. The vegetation and environment at the wulamulun site in the ordos plateau, inner Mongolia during MIS3 period. Acta Anthropol. Sin. 3, 60–69 (in Chinese with English abstract).
Li, Y.H., Sun, X.F., Bodin, E., 2014b. A macroscopic technological perspective on lithic production from the early to late pleistocene in the hanshui River Valley, central China. Quat. Int. 347, 148–162.
Li, Y.H., Zhou, Y.D., Sun, X.F., Li, H., 2016b. New evidence of a lithic assemblage containing in situ, late Pleistocene bifaces from the Houfang site in the Hanshui river valley, central China. C. R. Palevol. 17, 131–142.
Liu, J.X., Price, D.T., Chen, J.A., 2005. Nitrogen controls on ecosystem carbon sequestration: a model implementation and application to Saskatchewan. Canada. Ecol. Model. 186, 178–195.
Liu, T.S., Ding, M.L., 1984. A tentative chronological correlation of early human fossil horizons in China with the loess-deep sea records. Acta Anthropol. Sin. 2, 93–101 (in Chinese with English abstract).
Liu, T.S., 1985. Loess and the Environment. China Ocean Press, Beijing (in Chinese).
Liu, T.S., Ding, Z.L., 1999. Comparison of plio-pleistocene climatic changes in different monsoonal regions and implications for human evolution. Quat. Sci. 19, 289–298 (in Chinese with English abstract).
Liu, T.S., 1999. Loess stone artifact industry. In: Xu, Q.Q., Xie, F., Wang, J. (Eds.), International Symposium for the Celebration of Chinese Academician Jia Lanpo's 90th Birthday: New Advanced of Archaeology in Prehistory. Science Press, Beijing, pp. 52–62 (in Chinese).
Liu, X.B., Shen, G.J., Tu, H., Lu, C.Q., Granger, D.E., 2015. Initial $^{26}Al/^{10}Be$ burial dating of the hominin site Bailong cave in Hubei province, central China. Quat. Int. 389, 235–240.
Liu, Y., Feng, X.B., 2014. Hand-axe discovered at dishuiyan site in yunxian, hubei province. China cult. Relig. News 8, 1 (in Chinese).
Liu, Z., Otto-Bliesner, B.L., He, F., Brady, E.C., Tomas, R., Clark, P.U., Carlson, A.E., Lynch-Stieglitz, J., Curry, W., Brook, E., Erickson, D., Jacob, R., Kutzbach, J., Cheng, J., 2009. Transient simulation of last deglaciation climate evolution with a new mechanism for Bølling-Allerød warming. Science 325, 310–314.
Liu, Z.Y., Wen, X.Y., Brady, E.C., Otto-Bliesner, B., Yu, G., Lu, H.Y., Cheng, H., Wang, Y.J., Zheng, W.P., Ding, Y.H., Edwards, R.L., Cheng, J., Liu, W., Yang, H., 2014. Chinese cave records and the east Asia summer monsoon. Quat. Sci. Rev. 83, 115–128.
Lu, H.Y., Liu, X.D., Zhang, F.Q., An, Z.S., Dodson, J., 1999. Astronomical calibration of loess-paleosol deposits at Luochuan, central Chinese Loess Plateau. Paleogeogr. Paleoclimatol. Palaeoecoal. 154, 237–246.
Lu, H.Y., Miao, X.D., Sun, Y.B., 2002. Pretreatment methods and their influences on grain-size measurement of aeolian "red clay" in north China. Mar. Geol. Quat. Geol. 22, 129–135 (in Chinese with English abstract).
Lu, H.Y., Zhang, F.Q., Liu, X.D., Duce, R.A., 2004. Periodicities of palaeoclimatic variations recorded by loess-paleosol sequences in China. Quat. Sci. Rev. 23, 1891–1900.
Lu, H.Y., Zhang, H.Y., Wang, S.J., Cosgrove, R., Zhao, C.F., Stevens, T., Zhao, J., 2007. A preliminary survey on loess deposit in Eastern Qinling Mountains (Central China) and its implication for estimating age of the Pleistocene lithic artifacts.

Quat. Sci. 27, 559–567 (in Chinese with English abstract).
Lu, H.Y., Wang, X.Y., Li, L.P., 2010. Aeolian sediment evidence that global cooling has driven late Cenozoic stepwise aridification in central Asia. In: Clift, P.D., Tada, R., Zheng, H. (Eds.), Monsoon Evolution and Tectonics-climate Linkage in Asia, 342. Geo. Soc. London Spec Publ, pp. 29–44.
Lu, H.Y., Sun, X.F., Wang, S.J., Cosgrve, R., Zhang, H.Y., Yi, S.W., Ma, X.L., Wei, M., Yang, Z.Y., 2011a. Ages for hominin occupation in Lushi basin, middle of south Luohe River, central China. J. Hum. Evol. 60, 612–617.
Lu, H.Y., Zhang, H.Y., Wang, S.J., Cosgrove, R., Sun, X.F., Zhao, J., Sun, D.H., Zhao, C.F., Shen, C., Wei, M., 2011b. Multiphase timing of hominin occupations and the paleoenvironment in Luonan Basin, Central China. Quat. Res. 76, 142–147.
Lu, H.Y., Zhang, H.Y., Sun, X.F., Wang, S.J., Cosgrove, R., Shen, C., Zhang, W.C., Zhang, X.B., Wang, X.Y., Yi, S.W., 2012. Landform, loess deposit and paleoenvironmental changes in the south Luohe river (central China) during the hominin occupations. Quat. Sci. 32, 167–177 (in Chinese with English abstract).
Lu, H.Y., Zhuo, H.X., Zhang, W.C., Wang, S.J., Zhang, H.Y., Sun, X.F., Jia, X., Xu, Z.W., Wang, X.Y., 2017. Earth surface processes and their effects on human behavior in monsoonal China during the Pleistocene-Holocene epochs. J. Geogr. Sci. 27, 1311–1324.
Lu, X.H., Jiang, H., Liu, J.X., Zhang, X.Y., Jin, J.X., Zhu, Q.A., Zhang, Z., Peng, C.H., 2016. Simulated effects of nitrogen saturation on the global carbon budget using the IBIS model. Sci. Rep. 6, 39173.
Murray, A.S., Buylaert, J.P., Thomsen, K.J., Jain, M., 2009. The effect of preheating on the IRSL signal from feldspar. Radiat. Meas. 44, 554–559.
Pei, S.W., Guan, Y., Gao, X., 2008. A preliminary report on the excavation of the Pengjiahe paleolithic site in the Danjiangkou reservoir region. Acta Anthropol. Sin. 27, 95–110 (in Chinese with English abstract).
Pei, S.W., Li, X.L., Liu, D.C., Ma, N., Peng, F., 2009. Preliminary study on the living environment of hominids at the Donggutuo site, Nihewan Basin. Chin. Sci. Bull. 54, 2895–2901.
Pei, S.W., Niu, D.W., Guan, Y., Nian, X.M., Yi, M.J., Ma, N., Li, X.L., Sahnouni, M., 2015. Middle Pleistocene hominin occupation in the Danjiangkou reservoir region, central China: studies of formation processes and stone technology of Maling 2a site. J. Archaeol. Sci. 53, 391–407.
Ranov, V., 1995. The 'loessic Paleolithic' in south Tajikistan, central Asia: its industries, chronology and correlation. Quat. Sci. Rev. 14, 731–745.
Shaanxi Provincial Institute of Archaeology, Cultural Relics Administrative Committee of Shangluo District, Museum of Luonan County, 2007. Huashilang (I): the Paleolithic Open-air Sites in the Luonan Basin. Science Press, Beijing (in Chinese with English abstract).
Shaanxi Provincial Institute of Archaeology, Museum of Luonan County, 2008. Huashilang (II): Longyadong Paleolithic Cave Site in the Luonan Basin, China. Science Press, Beijing (in Chinese with English abstract).
Shackleton, N.J., An, Z.S., Dodonov, A.E., Gavin, J., Kukla, G.J., Ranov, V.A., Zhou, L.P., 1995. Accumulation rate of loess in Tadjikistan and China: relationship with global ice volume cycles. Wind Blown Sediments in the Quaternary Record 4, 1–6, 1995.
Shen, G., Gao, X., Gao, B., Granger, D.E., 2009. Age of Zhoukoudian Homo erectus determined with $^{26}Al/^{10}Be$ burial dating. Nature 458, 198–200, 2009.
Shen, G.J., 2012. In situ Cosmogenic Nuclide Burial Dating: recent progresses and prospects in Chronological studies of early hominin sites in China. Quat. Sci. 32, 382–387 (in Chinese with English abstract).
Shen, G.J., Wu, X.Z., Wang, Q., Tu, H., Feng, Y.X., Zhao, J.-X., 2013. Mass spectrometric u-series dating of Huanglong Cave in Hubei Province, central China: evidence for early presence of modern humans in eastern Asia. J. Hum. Evol. 65, 162–167.
Shen, Y.C., 1956. Geomorphology of the hanshui valley. Acta Geograph. Sin. 4, 296–323.
Stevens, T., Buylaert, J.-P., Murray, A.S., 2009. Towards development of a broadly-applicable SAR TT-OSL dating protocol for quartz. Radiat. Meas. 44, 639–645.
Sun, X.F., Mercier, N., Flagueres, C., Bahain, J.-J., Despriee, J., Bayle, G., Lu, H.Y., 2010. Recuperated optically stimulated luminescence dating of middle-size quartz grains from the Paleolithic site of Bonneval (Eure-et-Loir, France). Quat. Geochronol. 5, 342–347.
Sun, X., Lu, H.Y., Wang, S.J., Yi, S.W., 2012. Ages of liangshan paleolithic sites in Hanzhong Basin, central China. Quat. Geochronol. 10, 380–386.
Sun, X.F., Lu, H.Y., Wang, S.J., Yi, S.W., Shen, C., Zhang, W., 2013. TT-OSL dating of Longyadong Middle Paleolithic site and paleoenvironmental implications for hominin occupation in Luonan Basin (central China). Quat. Res. 79, 168–174.
Sun, X.F., Lu, H.Y., Wang, S.J., Cosgrove, R., Zhang, W.C., Yu, K.F., Zhuo, H.X., 2014. Age of newly discovered paleolithic assemblages at liuwan site Luonan basin, central China. Quat. Int. 347, 193–199.
Sun, X.F., Li, Y.H., Feng, X.B., Lu, C.Q., Lu, H.Y., Yi, S.W., Wang, S.J., Wu, S.Y., 2016. Pedostratigraphy of aeolian deposition near the yunxian man site on the Hanjiang river terraces at Yunxian basin, central China. Quat. Int. 400, 187–194.
Sun, X.F., Li, Y.H., Feng, X.B., Lu, C.Q., Lu, H.Y., Yi, S.W., Wang, S.J., Wu, S.Y., 2017a. Early human settlements in the southern Qinling Mountains, central China. Quat. Sci. Rev. 164, 168–186.
Sun, X.F., Jia, X., Lu, H.Y., Yi, S.W., Wang, X.Y., Xu, Z.W., Lei, F., Han, Z.Y., 2017b. A modified depositional hypothesis of the Hanjiang loess in the southern Qinling mountains, central China. Prog. Phys. Geogr. 41, 775–787.
Sun, X.F., Yi, S.W., Lu, H.Y., Zhang, W.C., 2017c. TT-OSL and post-IR IRSL dating of the Dali Man site in central China. Quat. Int. 434, 99–106.
Thomsen, K.J., Murray, A.S., Jain, M., Bøtter-Jensen, L., 2008. Laboratory fading rates of various luminescence signals from feldspar-rich sediment extracts. Radiat. Meas. 43, 1474–1486.
Wang, S.J., Huang, P.H., 2002. Stratigraphy and TL dating of Paleolithic sites in the Luonan basin, China. Acta Anthropol. Sin. 20, 229–237 (in Chinese with English abstract).
Wang, S.J., Zhang, X.B., Shen, C., Hu, S.M., Zhang, X.F., 2004. A study of lithic assemblages from 1995 excavation at Longyadong cave, Luonan basin, China. Acta Anthropol. Sin. 23, 93–110 (in Chinese with English abstract).
Wang, S.J., Shen, C., Hu, S.M., Zhang, X.B., Wang, C.F., Cosgrove, R., 2005. Lithic artefacts collected from open-air sites during 1995-1999 investigations in Luonan basin, China. Acta Anthropol. Sin. 24, 87–103 (in Chinese with English abstract).
Wang, S.J., Lu, H.Y., Zhang, H.Y., Zhao, J., Cosgrove, R., Yi, S.W., Sun, X.F., Wei, M., Garvey, J., Ma, X.L., 2008a. A preliminary survey of Paleolithic artifacts and loess deposit in the middle south Luohe river, eastern Qinling mountains, central China. Quat. Sci. 28, 988–999 (in Chinese with English abstract).
Wang, S.J., Lu, H.Y., Xing, L.D., 2014a. Chronological and typo-technological perspectives on the Palaeolithic archaeology in Lantian, central China. Quat. Int. 347, 183–192.
Wang, S.J., Lu, H.Y., 2014. Current perspectives on paleolithic archaeology in the upper Hanjiang river valley, central China. Acta Anthropol. Sin. 33, 315–328 (in Chinese with English abstract).
Wang, S.J., Sun, X.F., Lu, H.Y., Yi, S.W., Zhang, G.K., Xing, L.D., Zhuo, H.X., Yu, K.F., Wang, W., 2014b. Newly discovered paleolithic open-air sites in Hanzhong basin in upper valley of Hanjiang river and their ages. Acta Anthropol. Sin. 33, 125–136 (in Chinese with English abstract).
Wang, S.J., Lu, H.Y., 2016. Taphonomic and paleoenvironmental issues of the pleistocene loessic paleolithic sites in the qinling mountains, central China. Sci. China Earth Sci. 59, 1519–1528.
Wang, W., Mo, J.Y., Huang, Z.T., 2008b. Recent discovery of handaxes associated with tektites in the Nanbanshan locality of the Damei site, Bose basin, Guangxi, South China. Chin. Sci. Bull. 53, 878–883.
Wang, X.L., Wintle, A.G., Lu, Y.C., 2006. Thermally transferred luminescence in fine-rained quartz from Chinese loess: basic observations. Radiat. Meas. 41, 649–658.
Wang, X.L., Wintle, A.G., Lu, Y.C., 2007. Testing a single-aliquot protocol for recuperated OSL dating. Radiat. Meas. 42, 380–391.
Xia, W.T., Wang, S.J., Xia, N., Lu, H.Y., Wang, X.Y., Sun, X.F., Zhang, H.Y., Zhang, W.C., Zhuo, H.X., Xing, L.D., Yu, Q.Y., Feng, W.M., 2018. Lithic artifacts excavated from locality 3 of the Longgangsi site in Hanzhong Basin, Shaanxi province. Acta Anthropol. Sin. (in press).
Xia, Z.K., 1984. Preliminary observation of cenozoic beds in the Ankang Basin, Shaanxi. Geol. Shaanxi 2, 20–25.
Xia, Z.K., Zheng, G.W., Chen, F.Y., Liu, F.L., Guo, Y.Q., 1999. Paleolithic found in the loess layer of Luoyang. Quat. Sci. 19, 286 (in Chinese with English abstract).
Xia, Z.K., Chen, F.Y., Chen, G., Zheng, G.W., Xie, F., Mei, H.J., 2001. Environmental background of evolution from the paleolithic to Neolithic culture in Nihewan basin, north China. Sci. China Earth Sci. 44, 779–788 (in Chinese with English abstract).
Xia, Z.K., Li, D.C., Wang, Y.P., Qu, T.L., 2008. Environmental background of human activities during MIS 3 stage recorded in the Zhijidong cave site, Zhengzhou. Quat. Sci. 28, 96–102 (in Chinese with English abstract).
Xiao, J.L., Jin, C.Z., Zhu, Y.Z., 2002. Age of the fossil Dali Man in north-central China deduced from chronostratigraphy of the loess-paleosol sequence. Quat. Sci. Rev. 21, 2191–2198.
Xing, L.D., 2014. A Preliminary Study on the Stone Artifacts of Shizilukou Paleolithic Locality in Luonan Basin. Master's thesis, Central China.
Xu, X. H., Sun, X. F., Tu, H., Lu, Y. M., Zeng, Q. X., Cosmogenic $^{26}Al/^{10}Be$ Burial Dating of the Birth of the Han River (In Review).
Yang, X.Y., Xia, Z.K., Liu, T.S., 2005. Loess research and paleolithic archaeology in China. Quat. Sci. 25, 461–466 (in Chinese with English abstract).
Yi, S.W., Lu, H.Y., Stevens, T., 2012. SAR TT-PSL dating of the loess deposits in the horqin dunefield (northeastern China). Quat. Geochronol. 10, 56–61.
Yi, S.W., Buylaert, J.-P., Murray, A.S., Thiel, C., Zeng, L., Lu, H.Y., 2015. High resolution OSL and post-IR IRSL dating of the last interglacial-glacial cycle at the Sanbahuo loess site (northeastern China). Quat. Geochronol. 30, 200–206.
Zhang, B.S., 1981. Geomorphology of the qinling mountains. J. Northwest Uni. (Natural Sci. Ed.) 1, 78–84 (in Chinese with English abstract).
Zhang, D.J., Chen, F.H., 2013. A review of paleolithic environmental archaeology in north China. Mar. Geol. Quat. Geol. 4, 55–66 (in Chinese with English abstract).
Zhang, H.Y., Lu, H.Y., Jiang, S.Y., Vandenberghe, J., Wang, S.J., Cosgrove, R., 2012. Provenance of loess deposits in the eastern Qinling mountains (central China) and their implications for the paleoenvironment. Quat. Sci. Rev. 43, 94–102.
Zhang, J.-F., Li, Y.Y., Han, Y.-S., Wang, J.-K., Zhou, L.-P., 2018. Luminescence dating of weathered sediments from the Paleolithic site of Fengshuzui in northern Hunan province, China. Quat. Geochronol. (in press).
Zheng, Z., Zhang, X., Man, M.L., Wei, J.H., Huang, K.Y., 2016. Review and data integration of pollen-based quantitative paleoclimate reconstruction studies in China and adjacent areas. Quat. Sci. 36, 503–519 (in Chinese with English abstract).
Zhou, Z.Y., Wang, C.X., Gao, X., 2009. A preliminary report on the excavation of the Beitaishanmiao Paleolithic site at Danjiangkou, South China. Acta Anthropol. Sin. 28, 246–261 (in Chinese with English abstract).
Zhu, R.X., Hoffman, K.A., Potts, R., Deng, C.L., Pan, X.Y., Guo, B., Shi, C.D., Guo, Z.T., Yuan, B.Y., Hou, Y.M., Huang, W.W., 2001. Earliest presence of humans in northeast Asia. Nature 413, 413–417.
Zhu, R.X., An, Z.S., Potts, R., Hoffman, K.A., 2003. Magnetostratigraphic dating of early humans in China. Earth Sci. Rev. 61, 341–359.

Zhu, R.X., Potts, R., Xie, F., Hoffman, K.A., Deng, C.L., Shi, C.D., Pan, Y.X., Wang, H.Q., Shi, R.P., Wang, Y.C., Shi, G.H., Wu, N.Q., 2004. New evidence on the earliest human presence at high northern latitudes in northeast Asia. Nature 431, 559–562.

Zhu, Z.Y., Dennell, R., Huang, W.W., Wu, Y., Rao, Z.G., Qiu, S.F., Xie, J.B., Liu, W., Fu, S.Q., Han, J.W., Zhou, H.Y., Yang, T.P.O., Li, H.M., 2015. New dating of the *Homo erectus* cranium from lantian (gongwangling), China. J. Hum. Evol. 78, 144–157.

Zhu, Z.Y., Dennell, R., Huang, W.W., Wu, Y., Qiu, S.F., Yang, S.X., Rao, Z.G., Hou, Y.M., Xie, J.B., Han, J.W., Ouyang, T.P., 2018. Hominin occupation of the Chinese Loess Plateau scince about 2.1 million years ago. Nature 559, 608–612.

Zhuo, H.X., Lu, H.Y., Wang, S.J., Ahmad, K., Sun, W.F., Zhang, H.Y., Yi, S.W., Li, Y.X., Wang, X.Y., 2016. Chronology of newly-discovered paleolithic artifact assemblages in Lantian (Shaanxi province), central China. Quat. Res. 86, 316–325.